The α-galactosidase A deficient mouse as a model for Fabry disease and the effect of Gb3 depositions on peripheral nociceptive ion channel function

Die α-Galaktosidase A defiziente Maus als Modell für M. Fabry und der Effekt von Gb3-Ablagerungen auf die Funktion von peripheren nozizeptiven Ionenkanälen

Doctoral thesis for a doctoral degree

at the Graduate School of Life Sciences,

Julius-Maximilians-Universität Würzburg,

Section Neuroscience

submitted by

Lukas Hofmann

from

Schweinfurt

Würzburg 2017

Submitted on:

……..……..

Office stamp

Members of the *Promotionskomitee*:

Chairperson: Prof. Dr. Thomas Dandekar

Primary Supervisor: Prof. Dr. Nurcan Üçeyler

Supervisor (Second): Prof. Dr. Erhard Wischmeyer

Supervisor (Third): Prof. Dr. Carmen Villmann

Supervisor (Fourth): Prof. Dr. Claudia Sommer

Date of Public Defence: ……..……

Date of Receipt of Certificates: ……

Affidavit

I hereby confirm that my thesis entitled “The α-galactosidase A deficient mouse as a model for Fabry disease and the effect of Gb3 depositions on peripheral nociceptive ion channel function.” is the result of my own work. I did not receive any help or support from commercial consultants. All sources and / or materials applied are listed and specified in the thesis.

Furthermore, I confirm that the thesis has not yet been submitted as part of another examination process neither in identical nor in similar form.

Place, Date Signature

Eidesstattliche Erklärung

Hiermit erkläre ich an Eides statt, die Dissertation „Die α-galactosidase A defiziente Maus als Modell für M. Fabry und der Effekt von Gb3-Ablagerungen auf die Funktion von peripheren nozizeptiven Ionenkanälen“ eigenständig, d.h. insbesondere selbstständig und ohne Hilfe eines kommerziellen Promotionsberaters, angefertigt und keine anderen, als die von mir angegebenen Quellen und Hilfsmittel verwendet zu haben.

Ich erkläre außerdem, dass die Dissertation weder in gleicher noch in ähnlicher Form bereits in einem anderen Prüfungsverfahren vorgelegen hat.

Ort, Datum Unterschrift

Table of contents

Parts of the results presented in this thesis have been published:

Hofmann, L., et al., 2017. Affective and cognitive behavior in the alpha-galactosidase A deficient mouse model of Fabry disease. PLoS One. 12**,** e0180601.

The published manuscript and this thesis contain similar text passages in adapted form in some sections

1. Abstract

Fabry disease (FD) is an X-linked lysosomal storage disorder with intracellular accumulation of globotriaosylceramide (Gb3) due to α-galactosidase A deficiency. We studied α-galactosidase A knockout mice (GLA KO) as a model for sensory disturbance and pain in FD.

Pain associated behavior of young (3 months) and old (≥18 months) GLA KO mice and wildtype (WT) littermates in an inflammatory and a neuropathic pain model was investigated. Furthermore, affective and cognitive behavior was assessed in the naïve state and in an inflammatory pain model. Gene and protein expression of pain associated ion channels and Gb3 accumulation in dorsal root ganglion (DRG) neurons was determined. We also performed patch clamp analysis on cultivated DRG neurons and human embryonic kidney 293 (HEK) cells expressing voltage-gated-sodium channel 1.7 ($Na_v1.7$) as an in vitro model of FD. Intracellular Gb3 deposits were modulated using shRNA silencing of α-galactosidase A.

After intraplantar injection of complete Freund`s adjuvant (CFA) and chronic constriction injury (CCI) of the right sciatic nerve, old GLA KO mice did not develop heat and mechanical hypersensitivity in contrast to young GLA KO and old WT mice. Additionally, we found no relevant differences between genotypes and age-groups in affective and cognitive behavior in the naïve state and after CFA injection. Gene and protein expression analysis provided no explanation for the observed sensory impairment. However, cultured DRG neurons of old GLA KO mice revealed a marked decrease of sodium and I_h-currents compared to young GLA KO and old WT mice. DRG neurons of old GLA KO mice displayed substantial intracellular accumulation of Gb3 compared to young GLA KO and old WT mice. Similar to cultured neurons, sodium currents were also decreased in HEK cells treated with shRNA and consecutively increased intracellular Gb3 deposits compared to the control condition, but could be rescued by treatment with agalsidase-alpha.

Our study unveils that, similar to patients with FD, GLA KO mice display age-dependent sensory deficits. However, contrary to patients, GLA KO mice are also protected from hypersensitivity induced by inflammation and nerve lesion due to Gb3-dependent and reversible reduction of neuronal sodium- and I_h-currents. Our data provide evidence for direct Gb3-dependent ion channel impairment in sensory DRG neurons as a potential contributor to sensory dysfunction and pain in FD.

2. Zusammenfassung

Bei Morbus Fabry (M. Fabry) handelt es sich um eine X-chromosomal vererbte, lysosomale Speichererkrankung mit intrazellulärer Akkumulation von Globo-triaosylceramid (Gb3) aufgrund eines α-Galaktosidase-A Mangels. Um die Pathophysiologie des M. Fabry aufzuklären, untersuchten wir die α-Galaktosidase-A defiziente Maus (GLA KO) als Modell für sensible Wahrnehmungsstörungen und Schmerz.

Das schmerzassoziierte Verhalten von jungen (3 Monate) und alten (≥18 Monate) GLA KO Mäusen und Wildtyp (WT) Wurfgeschwistern wurde in einem Entzündungs- und einem neuropathischen Schmerzmodell untersucht. Zudem wurde das affektive und kognitive Verhalten im naiven Zustand und in einem Entzündungsschmerzmodell betrachtet. Auf molekularer Ebene wurden die Gen- und Proteinexpression von schmerzassoziierten Ionenkanälen und die Gb3-Akkumulation in Spinalganglionneuronen (dorsal root ganglion, DRG) bestimmt. Darüber hinaus wurden kultivierte DRG Neurone und humane embryonale Nierenzellen 293 (HEK) mittels Patch-clamp-Analyse elektrophysiologisch untersucht. Die HEK Zellen dienten als in vitro Modell für M. Fabry und exprimierten stabil den spannungsgesteuerten Natriumkanal 1.7 ($Na_v1.7$). Intrazelluläre Gb3 Ablagerungen wurden unter Verwendung von shRNA-Silencing der α-Galaktosidase A induziert.

Nach intraplantarer Injektion von complete Freund‘s Adjuvans (CFA) und chronic constriction injury (CCI) des rechten N. ischiadicus entwickelten alte GLA KO Mäuse, im Gegensatz zu jungen GLA KO und alten WT Mäusen, keine Überempfindlichkeit gegenüber Hitze und mechanischen Reizen. Darüber hinaus fanden wir keine relevanten Unterschiede zwischen Genotypen und Altersgruppen im affektiven und kognitiven Verhalten im naiven Zustand und nach Injektion von CFA. Gen- und Proteinexpressionsanalysen lieferten keine Erklärung für die sensible Beeinträchtigung. Jedoch zeigten kultivierte DRG Neurone von alten GLA KO Mäusen eine deutliche Abnahme der Natriumströme und der I_h Ströme im Vergleich zu jungen GLA KO und alten WT Mäusen. Außerdem wiesen DRG Neurone von alten GLA KO Mäusen eine verstärkte intrazelluläre Akkumulation von Gb3 im Vergleich zu jungen GLA KO und alten WT Mäusen auf. Ähnlich wie bei kultivierten Neuronen waren die Natriumströme in, mit shRNA behandelten HEK-Zellen, im Vergleich zu den Kontrollzellen ebenfalls verringert, konnten aber durch die Behandlung mit Agalsidase-alpha wiederhergestellt werden.

Unsere Studie zeigt, dass GLA KO Mäuse ähnlich wie Patienten mit M. Fabry altersabhängige sensible Veränderungen aufweisen. Im Gegensatz zu Patienten sind GLA KO Mäuse jedoch auch vor der Überempfindlichkeit geschützt, die durch eine Entzündung und Nervenläsion hervorgerufen wird. Unsere elektrophysiologischen Ergebnisse jedoch, deuten darauf hin, dass die Reduktion der Natrium- und I_h Ströme mit den veränderten Antworten auf die sensiblen Reize zusammenhängt. Diese Daten lassen auf eine Gb3 abhängige Ionenkanaldysfunktion in DRG Neuronen als potentiellen Faktor für sensible Fehlfunktion und Schmerz bei M. Fabry schließen.

3. Introduction

3.1 Fabry disease

3.1.1 Definition and epidemiology

Fabry disease (FD) is an X-linked hereditary lysosomal storage disorder (Zarate and Hopkin, 2008). It was first described independently by William Anderson and Johannes Fabry in 1898 as a skin disease based only on the typical angiokeratomas (Anderson, 1898; Fabry, 1898; Mehta et al., 2010) and unaware of other symptoms. It has long been considered that FD is caused by monogenetic mutations in the gene encoding the enzyme α-galactosidase A (α-Gal A) leading to reduced or complete loss of enzyme function (Schiffmann, 2009). Due to α-Gal A deficiency, the hydrolysis of alpha-galactosyl bonds of glycosphingolipids, which are often involved in the construction of cell membranes, is disrupted. This leads to the accumulation of glycosphingolipids, especially globotriaosylcermide (Gb3), in the lysosomes of various cell types of multiple organ systems (Germain, 2010). In this multi-organ disease, particularly the heart, the kidneys, and the nervous system are affected (Burlina et al., 2011) leading to a reduction of life expectancy (Germain, 2010). FD is the second most common lysosomal storage disorder after Gaucher`s disease (Mehta et al., 2010). The worldwide incidence varies from 1:40.000 to 1:117.000 (Meikle et al., 1999), with a high number of unreported patients. The prevalence rate also varies between countries with e.g. 1:3.100 for newborn boys in Italy (Spada et al., 2006), 1:1.250 in Taiwan (Hwu et al., 2009) and 1:3024 in Japan (Inoue et al., 2013).

3.1.2 Genetics

In 1967, Brady et al. first identified enzyme deficiency of the α-Gal A (Brady et al., 1967) as responsible for FD, but it took eleven years until Bishop et al. detected the gene encoding the α-Gal A at position Xq22.1 on the long arm of the X-chromosome (Bishop et al., 1988). The gene consists of 12.436 base pairs divided in seven exons (Schiffmann, 2009) with > 700 mutations known to date (http://fabry-database.org, Status: 10.04.2017). Missense or nonsense point mutations are most frequently reported (Germain, 2010), that are “private”, i.e. each family has an individual mutation. Due to X-linked inheritance men are mostly earlier and more severely

affected than women, however, random and skewed X-inactivation may cause any disease severity in women as well (Echevarria et al., 2015; Mehta et al., 2010; Toyooka, 2011). Contrary to this a recent study in a small cohort suggested that random X-inactivation may not be a main factor in disease variability (Biancini et al., 2017), thus further research is needed to investigate the main cause for FD symptom fluctuation.

3.1.3 Symptoms

FD may start in early childhood with typical Fabry-associated pain in up to 80% of the affected children (also see 3.2.2). Pain is mostly triggerable by e.g. feverous infections, heat, and physical activity (Germain, 2010) and is acrally located. Angiokeratomas can also be early signs of the disease. Organ manifestations typically start between 20 and 30 years of age and lead to a reduced life expectancy of an average of 50 years in male and 70 years in female patients (MacDermot et al., 2001a). These may include gastrointestinal symptoms, hypo- to anhidrosis, microalbumin- and proteinuria. Later, many patients develop renal insufficiency and mostly male patients may reach terminal renal failure by the age of 40 years (Lidove et al., 2007). In the further course of the disease heart and renal insufficiency progresses and the nervous system gets involved. Table 1 shows a summary of possible symptoms in FD.

Table 1: Symptoms of Fabry disease

Organ/ System	Symptoms
General	↓ Well being ↓ Exercise capacity ↓ Health-related quality of life Psychosocial limitations
Nervous system	Small fiber neuropathy Fabry-associated pain Polyneuropathy Cerebral ischemia
Heart	Left ventricular hypertrophy Arrhythmias Heart failure
Kidneys	↓Glomerular filtration rate Microalbuminuria Proteinuria Kidney failure
Skin	Angiokeratoma
Eyes	Cornea verticillata
Ears	Tinnitus Sudden hearing loss
Gastrointestinal tract	Diarrhea Abdominal pain Nausea

Adapted from (Burlina et al., 2011))

Besides pain and organ manifestations, FD patients also report of anxiety, depression, and cognitive impairment (Bolsover et al., 2014; Sigmundsdottir et al., 2014). Prevalence of anxiety in FD patients ranges between 20 and 37% and reaches up to 60% for depression (Balwani et al., 2009; Bolsover et al., 2014; MacDermot et al., 2001b). Additionally, patients may display mild and unprogressive impairment of cognitive functions (Lelieveld et al., 2015; Löhle et al., 2015; Sigmundsdottir et al., 2014). It is unknown, if the affective and cognitive symptoms in

FD are part of disease pathophysiology or a reactive process developing in the course of a life-threatening, chronic, and often painful disorder (Hofmann et al., 2017).

3.1.4 Diagnostics

Due to its rarity and variable clinical presentation, FD is an often under- or late diagnosed disease (Mehta et al., 2010) although several symptoms ("red flags" see Table 2) may be indicative. When FD is assumed in male patients, the biochemical evaluation of the α-Gal A activity in leukocytes or blood plasma is recommended. To confirm the diagnosis, genetic testing should be performed. In 20-30% of female patients enzyme activity can be normal. Therefore, a genetic analysis is mandatory in female FD patients. Upon confirmation of diagnosis, organ diagnostics should follow as well as a family screening (Rolfs et al., 2013; Sirrs et al., 2016).

Table 2: Typical symptoms in Fabry disease ("red flags")

Childhood	Adulthood	Family history
Inducible acral burning pain		Frequently occuring acral pain
Fabry crisis	Recurrent strokes at young age	Familial renal and heart disease
Recurrent feverish infections	Renal and / or cardiac insufficiency of unclear origin	Early deaths of unknown cause
Cornea verticillata	Cardiac arrhythmias of unknown cause	Hints for an X-linked inheritance

"Red flags", i.e. symptoms indicative of Fabry disease (adapted from (Üçeyler and Sommer, 2012))

3.1.5 Therapy

Since 2001 enzyme replacement therapy (ERT) is available for treatment of FD patients, which is intravenously and biweekly administered (Motabar et al., 2010). Currently two drugs are used: agalsidase-alpha and -beta (Tab. 3).

Table 3: Medication for Fabry disease

	Agalsidase-alpha	Agalsidase-beta
Trade name	Replagal®	Fabrazyme®
Production	Human skin fibroblasts	Ovarian cells of the chinese gold hamster
Dosis	0,2 mg/kg body weight	0,1 mg/kg body weight
Concomitant medication	Not necessary	Necessary (antihistaminic, antipyretic)

Adapted from (Schiffmann et al., 2017)

ERT is recommended early in disease course to avoid organ manifestations; it reduces cardiac mass and renal Gb3 accumulation, but data on its effect on the nervous system is conflicting (Biegstraaten et al., 2015). Additionally, ERT is time consuming, expensive, and can potentially induce immune reactions against the recombinant enzyme (Üçeyler and Sommer, 2012). Because of these limitations and disadvantages, there is intensive research ongoing for alternative treatment options. In 2016, the European Medicines Agency approved Migalastat (Galafold®) as the first oral drug for FD. This chaperone selectively binds to distinct mutation sites of the misfolded α-Gal A enzyme. By now there are 269 mutations which are responsive to treatment with Migalastat ((Germain et al., 2016);www.galafoldamenabilitytable.com). Migalastat stabilizes and restores enzyme activity and enhances Gb3 degradation with consecutive organ protection and functional improvement (Hughes et al., 2017). As for remaining symptoms, adjunctive therapy is recommended as needed (Üçeyler and Sommer, 2012). Besides organ pathology, Fabry-associated pain is the main limitation of health related quality of life. However, symptomatic analgesic treatment is mostly hampered by potential side effects in FD patients with multimorbidities. Also, the underlying mechanisms of pain pathophysiology in FD are incompletely understood, which limits the generation of specific analgesic drugs.

3.2 Nervous system involvement in FD and pain

3.2.1 Central nervous system (CNS)

Gb3 depositions in cerebral endothelial cells have been associated with stroke at young age in FD (Sims et al., 2009; Toyooka, 2011). The relative risk for cerebral stroke in the USA is 12.2 fold higher in FD patients compared to healthy controls in the age-group of 35 to 45 years (Sims et al., 2009), while the mean age at first stroke among male FD patients is 39.8 years compared to 76 years in the general population (Carandang et al., 2006; Sims et al., 2009). To date no cases of vertebral dissection or spinal cord infarction have been documented in FD patients (Kolodny et al., 2015). As another effect of FD on the CNS, so called white matter lesions (WML) can be observed on cerebral MRI scans of FD patients which are of so far unknown biological relevance and pathophysiology (Fellgiebel et al., 2014). Quantitative WML analysis might be a potential opportunity to asses biomarkers for the development of individual and effective therapies (Inoue et al., 2013). Additionally, FD patients frequently report on anxiety, depression, and cognitive impairment (Bolsover et al., 2014; Sigmundsdottir et al., 2014).

3.2.2 Peripheral nervous system

In the peripheral nervous system (PNS) of FD patients, mostly the thinly-myelinated Aδ and unmyelinated C fibers are affected. This may lead to small fiber neuropathy (SFN) with a reduction or complete loss of the intraepidermal innervation (Burlina et al., 2011; Üçeyler et al., 2011). Functional impairment is reflected by elevated thermal perception thresholds in the quantitative sensory testing (QST) (Maag et al., 2008; Üçeyler et al., 2011), reduced potential amplitudes of pain-related evoked potentials elicited by electrical stimulation of A-delta fibers in male FD patients, (Üçeyler et al., 2013), and reduced corneal innervation (Tavakoli et al., 2009). Clinically, patients report of FD-associated pain, which presents with diverse phenotypes (Üçeyler et al., 2014) and is one of the earliest symptoms. Neuropathic pain is defined as pain arising as a direct consequence of a lesion or disease affecting the somatosensory system (Treede et al., 2008). In contrast, nociceptive pain is caused by activation of nociceptors e.g. by heat, cold or chemicals. FD pain is predominantly assumed to be neuropathic (Politei et al., 2016) and can be triggered by e.g. feverish infections, heat or physical activity and occurs in up to 80% of

children with FD (Burlina et al., 2011; Germain, 2010). Most FD patients report of pain attacks with acral burning pain located at the soles and the palms. These attacks are inducible by typical triggers, but can be attenuated when the triggering stimulus is avoided. The inducible Fabry crisis is an extreme form of FD pain. Fabry crises occur episodically, spread from the distal extremities to the proximal parts of the body, and can last up to several days. In contrast to pain attacks, avoiding the trigger or analgesic medication has no or little effect on the Fabry crisis. Additionally, some FD patients report of evoked pain like hyperalgesia or allodynia at their extremities (Üçeyler and Sommer, 2012). Few patients suffer from permanent acral pain, which is mostly burning or associated with tingling paresthesias and is independent from any trigger. Usually pain intensity decreases with aging, but pain onset in adulthood or even after treatment initiation can be observed (Zarate and Hopkin, 2008).

3.3 Potential pathomechanisms of Fabry-associated pain

Fabry-associated pain is one of the main limitations of patients` health related quality of life (Germain, 2010; Üçeyler et al., 2014), but the underlying pathomechanism is incompletely understood. Based on histopathological findings, it is assumed that Gb3 depositions in DRG neurons may lead to pathological changes in the transduction of nociceptive signals and thus cause pain (Gadoth and Sandbank, 1983; Kaye et al., 1988; Schiffmann, 2009). In a mouse model of FD the authors showed that the expression and function of the thermal sensitive transient receptor potential vanilloid 1 (TRPV1) channel was increased compared to controls (Lakoma et al., 2016b). Choi et al. reported that Gb3 and its derivative lyso-Gb3 induce increased calcium influx in cultured DRG neurons of Bl6/J mice, which might result in pain (Choi et al., 2015). Another hypothesis is that Gb3 and its metabolites are potentially neurotoxic and might induce apoptosis (Jeyakumar et al., 2002; Shen et al., 2008) which might contribute to SFN and pain.

3.4 Models of FD

3.4.1 Mouse models of FD

The pathophysiology of FD was first investigated in post mortem tissue (Gadoth and Sandbank, 1983; Kaye et al., 1988). Meanwhile, several mouse models have been developed to investigate disease pathophysiology.

3.4.1.1 The α-Gal A deficient mouse

In 1997 Ohshima et al. created the α-Gal A deficient mouse (GLA KO) by targeting gene disruption in mouse embryonic cells (Ohshima et al., 1997). The complete loss of enzyme function in the GLA KO mouse was confirmed by analysis of enzyme activity in different tissues and cultivated fibroblasts (Ohshima et al., 1997). Additionally, it was shown that GLA KO mice develop Gb3 accumulations in different body fluids and tissues similar to FD patients (Bangari et al., 2015; Takenaka et al., 2000), but without reduced life expectancy (Marshall et al., 2010). To study the comparability of the human phenotype and the mouse model, pain associated behavior, molecular, and histological characteristics of the GLA KO mouse were investigated. It was shown that the GLA KO mouse age-dependently develops thermal hyposensitivity, while remaining hypersensitive for mechanical stimuli without motor dysfunction in both genders (Lakoma et al., 2014; Rodrigues et al., 2008; Üçeyler et al., 2016). Furthermore, histological examination revealed Gb3 accumulations in DRG neurons with increased neuron size compared to control mice (Bangari et al., 2015; Marshall et al., 2010). Additionally, GLA KO mice displayed reduced intraepidermal nerve fiber density and increased Nav1.8 and TRPV1 protein expression in footpad skin (Lakoma et al., 2014). Lakoma et al. also reported that TRPV1 currents were increased in cultivated DRG neurons after treatment with capsaicin compared to control mice (Lakoma et al., 2016b), which may potentially underlie Fabry-associated pain. Another recent study reported similar alterations in the conduction velocity of nociceptors in FD patients using microneurography and the GLA KO mouse using ex vivo skin–nerve preparations (Namer et al., 2017). The authors also observed reduced Na_v and voltage-gated calcium current conductance in the GLA KO mouse DRG neurons, which may contribute to reduced sensitivity against noxious thermal stimuli in GLA KO mice and FD patients respectively (Namer et al., 2017).

3.4.1.2 G3Stg/GLA deficient mouse

The GLA KO mouse has a rather mild sensory phenotype without any α-Gal A enzyme function (Marshall et al., 2010; Ohshima et al., 1997). This is in contrast to the situation in FD patients where residual α-Gal A enzyme activity can be preserved. The murine Gb3 synthesis capacity might be lower than in humans, thus, Taguchi et al. hybridized the GLA KO mouse with a mouse strain additionally expressing the human Gb3 synthase (G3Stg mouse) (Shiozuka et al., 2011; Taguchi et al., 2013), resulting in the G3Stg/GLA deficient mouse. Gb3 serum concentration and organ accumulation, especially in the heart, the renal system, and the CNS, is substantially increased in this mouse strain and mice display renal dysfunction and reduced life expectancy (Taguchi et al., 2013). This mouse model thus leads to early and severe symptoms.

3.4.2 In vitro models of FD

To investigate consequences of FD on specific cell types, several *in vitro* models have been used. Especially skin fibroblasts obtained from FD patients were assessed qualitatively and quantitatively for Gb3 deposits (Askari et al., 2007; Keslova-Veselikova et al., 2008; Lakoma et al., 2016a). Peripheral blood mononuclear cells were used to study the effects of Gb3 accumulation on the immune response (De Francesco et al., 2013). Since the comparison of the human and murine phenotype is difficult, induced pluripotent stem cells from reprogrammed patient derived fibroblasts were generated (Nakagawa et al., 2008), which could then be further derived to human neuronal cells, e.g. nociceptors from FD patients (Kawagoe et al., 2013).

3.5 Pain related ion channels

Pain perception is an essential physiological function to provide protection from injury. Peripheral nerve endings of nociceptors are activated by chemical, mechanical or thermal stimuli. This initiates action potentials, which are conducted across the axons of these primary afferent fibers through the DRG into the synaptic sites in the spinal dorsal horn and further to the brain. Neuronal ion channels are responsible for action potential initiation and propagation (Waxman and Zamponi, 2014). After nerve injury, ion channel expression and function may be maladaptively modified, which can cause hyperexcitability in pain signaling neurons resulting in acute or chronic neuropathic pain. As described previously, Gb3 accumulation in DRG neurons of FD

patients might cause Fabry-associated pain by altering ion channel expression and/or function (Gadoth and Sandbank, 1983; Kaye et al., 1988; Schiffmann, 2009).

3.5.1 Transient receptor potential vanilloid 1 (TRPV1)

The family of thermosensitive transient receptor potential (TRP) cation channels are non-selective cation channels, which are sensitive to noxious temperatures, as well as mechanical and chemical stimuli (Bourinet et al., 2014). By stimulation of these TRP channels, influx of calcium and sodium ions results in membrane depolarization and action potential propagation. These channels play an important role in the somatosensory perception (Bourinet et al., 2014), while increased expression or function is often associated with inflammatory and neuropathic pain (Salat et al., 2013). One subclass of TRP channels are the vanilloid type channels. Within this group of six different subtypes, the TRPV1 channel, receptor for the vanilloid irritant capsaicin, seems to play an essential role in inflammatory and neuropathic pain. TRPV1 is expressed in small to medium diameter DRG neurons and nociceptors as well as in CNS (Caterina et al., 1997) and is characteristically sensitive to heat (≥43°C), acidosis, capsaicin, mechanical stimuli, and pro-inflammatory mediators (Bourinet et al., 2014; Tominaga, 2007). It has been shown that there is no heat hyperalgesia after inflammation in TRPV1 KO mice, which suggests a regulatory role in temperature dependent hypersensitivity mechanisms (Breese et al., 2005; Caterina et al., 2000). Additionally, temperature thresholds of TRPV1 can be lowered by pro-inflammatory mediators (Bourinet et al., 2014) resulting in increased heat sensitivity.

3.5.2 Hyperpolarization-activated cyclic nucleotide-gated ion channel 2 (HCN2)

Hyperpolarization-activated cyclic nucleotide-gated (HCN) channels are a family of four different subtypes (1-4), which are all expressed in DRG neurons (Matsuyoshi et al., 2006) and play an important role in neuronal excitability and action potential frequency (I_h currents) (Benarroch, 2013). Especially HCN2 seems to play a pivotal role in small nociceptors as an action potential pacemaker under neuropathic and inflammatory pain conditions (Acosta et al., 2012; Emery et al., 2011; Smith et al., 2015). Papp et al. reported an increase of HCN2 expression in the spinal dorsal horn after inflammation induced by complete Freund`s adjuvant (CFA) (Papp et al., 2010). In contrast, inhibition of HCN2 alleviated heat hyperalgesia after nerve inflammation

(Richards and Dilley, 2015). Additionally, HCN2 deficient mice displayed normal pain perception, but were protected from heat hyperalgesia induced by inflammation and did not develop neuropathic pain (Emery et al., 2011).

3.5.3 Voltage-gated sodium channels

Voltage gated sodium channels (Na_v) are responsible for action potential generation and propagation. The Na_v family consists of nine subtypes ($Na_v1.1$–1.9), which are expressed in different neuronal cells of the CNS and PNS, cardiac cells, skeletal muscle cells, and gastrointestinal smooth muscle cells. $Na_v1.7$, $Na_v1.8$, and $Na_v1.9$ are particularly found in small nociceptive neurons and are regulators of neuronal excitability (Dib-Hajj et al., 2009). Increased expression and/or function especially of $Na_v1.7$ and $Na_v1.8$ may be associated with changes in neuronal activity, resulting in several pain syndromes and congenital insensitivity to pain (Brouwer et al., 2014; Lai et al., 2003; Waxman et al., 1999).

3.5.3.1 $Na_v1.7$

In several studies $Na_v1.7$ was identified as a key player in neuropathic pain (Waxman and Zamponi, 2014). Gain-of-function mutations in the encoding gene of the channel were detected as a cause of pain in primary erythromelalgia (Dib-Hajj et al., 2005; Yang et al., 2004) and paroxysmal extreme pain disorder (Fertleman et al., 2006). Additionally, rat DRG neurons transfected with gain-of-function mutated human $Na_v1.7$ channels displayed impaired neurite integrity, resulting in time-dependent axon degeneration *in vitro* (Persson et al., 2013; Rolyan et al., 2016). In contrast to the effects of gain-of-function mutations, heat sensitivity was unchanged after burn injury in $Na_v1.7$ nociceptor-specific knockout mice (Nassar et al., 2005). This is similar to humans, where loss-of-function mutations may lead to congenital insensitivity to pain (Cox et al., 2006).

3.5.3.2 $Na_v1.8$

Together with $Na_v1.7$, $Na_v1.8$ is also important for neuronal nociceptive function (Waxman and Zamponi, 2014). Neurons expressing $Na_v1.8$ are essential in mechanical, inflammatory, and cold pain perception (Brouwer et al., 2014). Gain-of-function mutations of the encoding gene can also lead to age-dependent SFN (Faber et al., 2012) and hyperexcitable DRG neurons with increased firing rate and spontaneous activity (Brouwer et al., 2014; Faber et al., 2012). In contrast, $Na_v1.8$ knock-out mice displayed moderate hypoalgesia upon noxious thermal and mechanical stimulation (Lai et al., 2003).

3.6 Aims of the study

Based on the findings of the human and murine FD sensory phenotype and pain-associated ion channel contribution, we hypothesized that Gb3 accumulation in DRG neurons may be causally linked with FD-associated pain, sensory disturbance, and nerve fiber degeneration. The following questions were addressed in this thesis to provide a potential mechanism for small fiber degeneration and pain in FD:

- Does the GLA KO mouse display differences in pain-, affective, and cognitive behavior compared to wildtype littermates modeling the FD phenotype?
- Are there differences in gene and protein expression of pain related ion channels in DRG neurons of GLA KO mice underlying the respective behavioral phenotype?
- Do electrophysiological alterations, linked with the GLA KO mouse, provide hints for a potential mechanism leading to SFN and pain in FD?

4. Material and methods

4.1 Ethics statement

Our study was approved by the Bavarian state authorities (Regierung von Unterfranken, # 54/12). Animal use and care were in accordance with institutional guidelines. Mice were held in the animal facilities of the Department of Neurology, University of Würzburg. They were fed standard chow (commercially prepared complete diet) and had food and water access ad libitum.

4.2 Mice, genotyping, and study groups

We investigated 37 male and 38 female GLA KO mice carrying a targeted disruption of the α-GAL gene as previously described (Ohshima et al., 1997) and 37 male and 38 female WT littermates of C57Bl/6N background for pain-associated behavior. Genotypes were identified after purification of genomic DNA from ear biopsies using the DNeasy blood&tissue kit (Qiagen, Hilden, Germany) according to the manufacturer's instructions. The Kapa2G fast PCR Kit (Kapa Biosystems, Wilmington, USA) was used to determine the genotypes by conventional PCR (respective primer sequences listed in Appendix 8.4). Additionally, we assessed 32 male GLA KO mice and 32 male inbred WT littermates for affective and learning behavior. GLA KO breeder pairs had been obtained with kind permission of Prof. A. Kulkarni (National Institute of Health, Bethesda, USA) (Ohshima et al., 1997). Mice were separated into two age-groups of young (3 months) and old (12-24 months) animals.

4.3 Pain models

As a model for inflammatory pain, the right hind paw of GLA KO and WT mice was injected with complete Freund`s adjuvant (CFA, Sigma-Aldrich, Taufkirchen, Germany) i.pl. Ten µl CFA (concentration: 20 pg/µl, dilution: 1:100.000) were applied under isoflurane anesthesia (CP-Pharma, Burgdorf, Germany). Ten µl of sodium chloride (NaCl 0.9%, Braun, Melsungen, Germany) was injected into the right hind paw of each control cohort for comparison.

To model neuropathic pain, mice of the old age-group received a chronic constriction injury (CCI) of the right sciatic nerve (Bennett and Xie, 1988; Sommer and Schäfers,

1998) or Sham surgery. The right sciatic nerve was exposed, while mice were anesthetized with isoflurane. Three ligatures (7-0 prolene, Ethicon, Norderstedt, Germany) with a distance of one mm each were loosely tied around the nerve proximal to its trifurcation until the ipsilateral hind paw flicked shortly.

4.4 Behavioral tests

All behavioral tests were performed by the same experienced investigator blinded to the genotype.

4.4.1 Pain behavioral tests

Tests were started after at least one week of adaptation to the testing environment and the different test devices. All mice were examined three times each with a test interval of 1-2 weeks before interventions. Pain behavioral tests and locomotor activity were performed following the algorithms shown in Fig. 1.

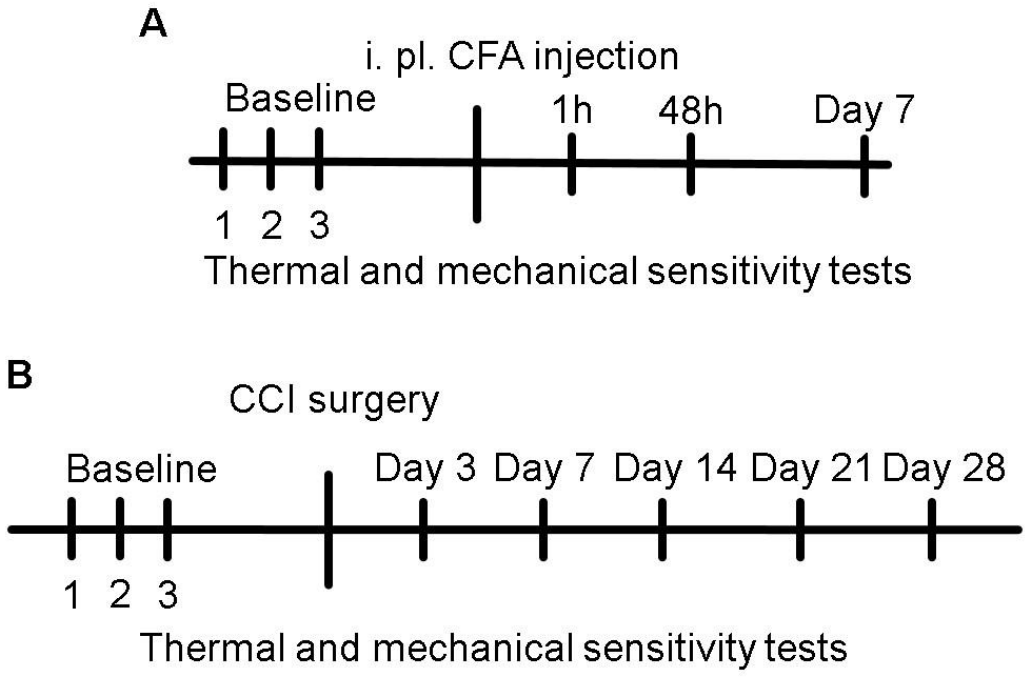

Figure 1: Experimental design for pain associated behavior in two inflammatory and a neuropathic pain model

Timelines show the test sequences at baseline and after i.pl. injection of complete Freund`s adjuvant (CFA) into the right hind paw (A), after chronic constriction injury (CCI) of the right sciatic nerve (B). Pain associated behavior and locomotor activity was investigated in young (3 months) and old (12-24 months) α-GAL deficient (GLA KO) and wildtype (WT) littermate male mice after CFA and LPS injection and in old GLA KO mice and WT littermates after CCI surgery. For both pain models, mice were tested in the naïve state for baseline values. Thermal and mechanical thresholds were obtained

at one hour, 48 hours, and seven days post CFA injection (A) and three to 28 days post CCI (B). Locomotor activity was also tested in the naïve state, six, and 24 hours after i.p. LPS injection (C).

4.4.1.1 Heat withdrawal latencies

To determine heat withdrawal latencies, the Hargreaves method with a standard Ugo Basile Algometer (Comerio, Italy) was applied (Hargreaves et al., 1988). Mice surrounded by individual acrylic glass boxes were positioned on a glass surface and, after 60 minutes of adaptation, a radiant heat stimulus (25 IR) was placed under the plantar surface of the hind paw. The paw withdrawal latency was measured automatically. To avoid tissue damage, stimulus cut-off was set at 16 seconds. Both hind paws were consecutively tested three times.

4.4.1.2 Cold withdrawal latencies

Cold withdrawal latencies were detected applying a cold plantar test (Brenner et al., 2012). Mice surrounded by individual acrylic glass boxes were placed on a glass surface (1/4´´) and dry ice filled in a syringe was pressed against the glass at the plantar surface under the hind paw. Time until paw withdrawal was recorded. To avoid tissue damage, a stimulus cut-off time of 20 seconds was set for stimulus application

4.4.1.3 Mechanical withdrawal thresholds

The von-Frey test based on the up-and-down-method (Chaplan et al., 1994) was used to determine mechanical withdrawal thresholds. Mice individually surrounded by acrylic glass boxes were positioned on a wire mesh 60 minutes for adaption. After this, the plantar surface of the hind paws was touched with a von-Frey filament (beginning at 0.69 g). Upon paw withdrawal the next thinner von-Frey filament was applied. If no paw withdrawal was observed, the next thicker von-Frey filament was used. Both hind paws were tested six times. The 50% withdrawal threshold (i.e. force of the von-Frey hair to which an animal reacts in 50% of the administrations) was calculated.

4.4.2 Affective and cognitive behavior

One male cohort of both genotypes and age-groups was investigated for affective and learning behavior in the naïve state and another cohort one and 48 hours after i.pl. injection of 10 µl of CFA to the right hind paw. Tests were applied following the algorithm shown in Fig. 2. All tests were video recorded for off-line analysis. Mice were housed in a reversed light-dark cycle (light cycle: 7 p.m.-7 a.m.; dark cycle: 7 a.m.-7 p.m.) and were tested during their active phase.

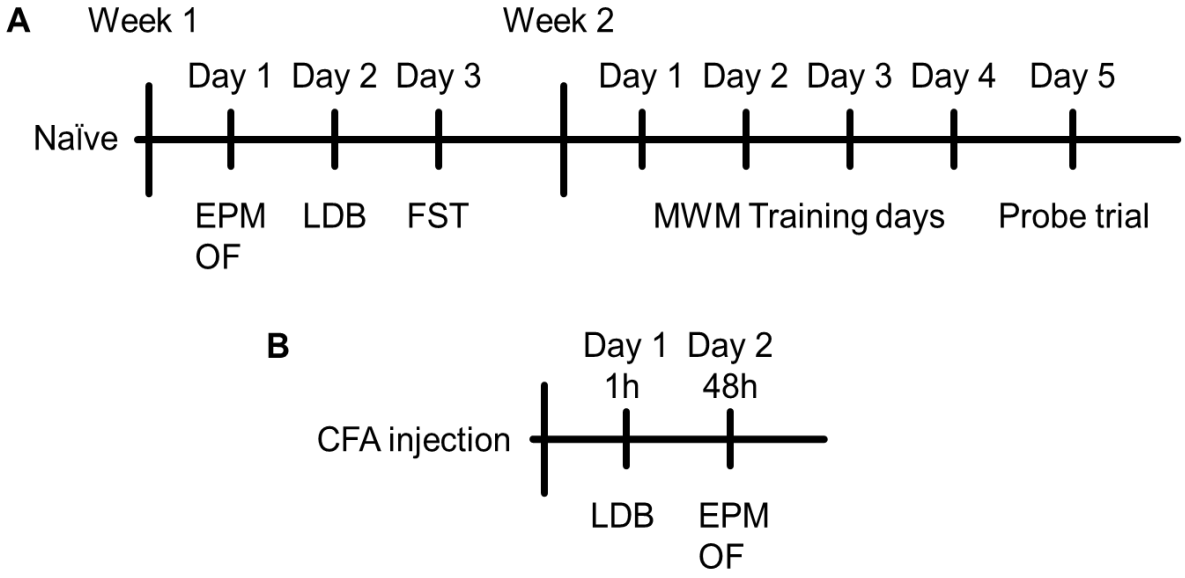

Figure 2: Experimental design for affective and learning behavior

Timelines show the test sequences at baseline and after i.pl. injection of complete Freund`s adjuvant (CFA) into the right hind paw. Anxiety- and depression-like behavior was investigated in young (3 months) and old (12-24 months) α-GAL deficient (GLA KO) and wildtype (WT) littermate male mice in the naïve state on three consecutive days of the first test week and learning behavior on five days of the second test week (A). (B) Additionally, anxiety-like behavior was tested one and 48 hours after CFA injection when pain maximum was assumed (Allen et al., 2003; Yang et al., 2009). Abbreviations: EPM=elevated plus maze; FST=forced swim test; LDB=light-dark box; MWM=Morris water maze; OF=open field test.

4.4.2.1 Anxiety tests

To assess anxiety-like behavior, the elevated plus maze (EPM) (Pellow et al., 1985), the light-dark box (LDB) test (Crawley and Goodwin, 1980), and the open field test (OF) (Prut and Belzung, 2003) were performed. These three tests were chosen to investigate the expected range of intra-individual outcome variation (Ramos, 2008). Mice were tested five minutes each. Behavioral parameters were recorded in a black box under infrared light to avoid interference with the investigator and other mice.

The EPM apparatus consisted of two opposite open arms (66.5 cm) and two closed arms (65.5 cm), separated by a junction area. Mice were placed individually in the middle of the apparatus, facing an open arm. The total time spent in open arms was determined.

The LDB consisted of an illuminated (40 cm x 20.5 cm) and a dark compartment (40 cm x 19.5 cm), separated by an opening through which mice could switch between the compartments. Each mouse was first placed in the light box and was allowed to explore the apparatus freely. The percentage of time spent in the light box and the number of entries into the dark box were recorded.

The OF box (40 cm x 40 cm) was divided into two areas, the center zone (20 cm x 20 cm) and the surrounding area. Mice were placed individually in the middle of the center zone and the time spent in the center zone and total distance travelled was measured.

4.4.2.2 Depression-like behavior

Using the forced swim test (FST) (Porsolt et al., 1977), depression-like behavior of naïve young GLA KO and WT mice was determined. Old mice were spared due to physical exhaustion in the stressful experimental situation. Mice were placed in a glass cylinder partially filled with water (diameter: 11.5 cm; water height: 12.5 cm; temperature: 20°C ±2°C). Within a six minute period, mouse behavior was observed for five minutes. Water level was selected to force mice to swim or to float without touching the bottom. Time spent immobile was measured.

4.4.2.3 Learning behavior

The Morris water maze (MWM) (Morris, 1984) was used to test the learning behavior. A plastic cylindrical pool (diameter: 118. 5 cm) was filled with opaque water (temperature: 20°C ±2°C) just covering a hidden platform (diameter: 8 cm). The pool was divided into four sections and the platform was placed in the south-east (target zone) quadrant. Mice were given four sessions of swimming with four different starting points, located in the middle of each of the four quadrants, on each of four consecutive training days. Time spent to reach the platform was measured. If the platform was not reached within 60 seconds, mice were placed on the platform for 15 seconds by the experimenter. At day five (probe trial) a new starting point was selected, the platform was removed, and mice were tracked for one minute. Time

spent to find the platform during the training days for each mouse was measured and daily average of each genotype and age-group was calculated. On the probe trial, time until first entry into the target zone and time travelled in the target zone was measured.

4.4.2.4 Video processing

Acquired videos were analyzed using the ANY-maze video tracking system (system version: 4.99m, Stoelting, Wooddale, IL, USA).

4.5 Tissue collection

To dissect lumbar DRG L3 and L5 from the right side using a dissection microscope (Zeiss, Oberkochen, Germany) for quantitative real-time PCR (qRT-PCR), mice were sacrificed in deep isoflurane anesthesia. Material was obtained at baseline and seven days after i.pl. CFA injection; tissue was flash-frozen in liquid nitrogen for storage at -80°C before further processing. L4 DRG was collected for immunohistochemistry at baseline and seven days after intervention (see below). Material was embedded in OCT medium (optimal cutting temperature; TissueTek®, Sakura Finetek, Staufen, Germany) and stored at -80°C before further processing. For neuronal cell cultures all DRG of the spinal cord available were dissected (see below).

4.6 Gene expression analysis

To homogenize frozen DRG samples a Polytron PT 3100 homogenizer (Kinematica, Luzern, Switzerland) was used. Total RNA was isolated with TRIzol reagent (Life Technologies, Carlsbad, CA, USA) following the manufacturer's instructions. RNA concentration was quantified spectrophotometrically with the NanoPhotometer Pearl® (Implen, Munich, Germany). 500 ng of RNA were then reverse transcribed using TaqMan Reverse Transcription Reagents (Applied Biosystems, Darmstadt, Germany). The PCR reaction additionally contained 10x Reaction Buffer (10 µl), 10 mM dNTPs (20 µl), 25 mM MgCl2 (22 µl), Random Hexameres (5 µl), RNAse Inhibitor (2 µl) and 50 U/µl Multiscribe Reverse Transcriptase (6.25 µl), to complete the reaction volume of 100 µl. PCR reactions were performed in the 96-well GeneAmp® PCR System 9700 cycler with following cycler conditions: 10 min, 38°C; 60 min, 48°C; 25 min, 95°C. Five µl of cDNA per sample were then assessed with

qRT-PCR using TaqMan Universal Master Mix and the following target specific pre-designed mouse TaqMan Gene Expression Assays (Applied Biosystems, Darmstadt, Germany; Assay-IDs in brackets): transient receptor potential vanilloid 1 (TRPV1) (Assay-ID: Mm01246302_m1), potassium/sodium hyperpolarization-activated cyclic nucleotide-gated ion channel 2 (HCN2) (Mm00468538_m1), voltage-gated sodium channel 1.7 ($Na_v1.7$) (Mm00450762_s1), and voltage-gated sodium channel 1.8 ($Na_v1.8$) (Mm00501467_m1). 18s rRNA (Hs99999901_s1) was used as an endogenous control. Relative gene expression was calculated with the $2^{-\Delta\Delta Ct}$ method.

4.7 Immunohistochemistry

Ten µm DRG cryosections were prepared with a cryostat (Leica, Bensheim, Germany). Immunoreaction was performed using antibodies against TRPV1 (goat, 1:500, Santa Cruz, cat# SC-12498; Santa Cruz, CA, USA), HCN2 (rabbit, 1:200, Alomone Labs, cat# APC-030; Jerusalem, Israel), $Na_v1.8$ (rabbit, 1:100, Chemicon, cat# AB9274 , Temecula, CA, USA), and CD77 (i.e. Gb3, rat, 1:250, Bio-Rad, cat# MCA579; Hercules, CA, USA). Goat anti-rabbit IgG and rabbit anti-goat IgG labelled with cyanine 3.18 fluorescent probe (Cy3, 1:50, Amersham; Piscataway, NJE, USA) and Alexa Fluor 488 goat anti-rat IgM (1:300; Jackson Laboratory; Bar Habor, MA, USA) were used as secondary antibodies. Negative controls were prepared by omitting the primary antibody and gave no signals. Total number of neurons per DRG were assessed manually (Axiophot 2 microscope, Zeiss, Oberkochen, Germany) using Spot Advanced Software (Windows Version 5.2) and Fiji software (ImageJ 1.50g, Wayne Rasband, National Institute of Health, USA) (Schindelin et al., 2012). Percentage of immunoreactive neurons relative to the total number of neurons was calculated by an observer unaware of the genotype, to quantify ion channel expression and Gb3 positive cells. Additionally, five different $Na_v1.7$ polyclonal antibodies were tested (anti-rabbit, Alomone Labs: cat# ASC-008; anti-rabbit, cat# ASC-027; anti-ginuea pig, cat# AGP-057, Jerusalem, Israel), (anti-mouse, Abcam, cat# ab85015, Camebridge, UK), and rabbit anti-Nav1.7 (Y083, generated from rat a.a. sequence 514–532, Center for Neuroscience and Regeneration Research, Yale Medical School and Veterans Affairs Hospital, West Haven, CT, USA). Also, DRG of a young and old GLA KO, and an old WT mouse each were collected in 4% paraformaldehyde (Merck Millipore, cat# 1.04005; Billerica, MAS, USA) in glutaraldehyde (Serva, cat# 23115, Heidelberg, Germany). To obtain 0.5 µm semithin

plastic sections an Ultramicrotome (Leica EM UC7, Leica Microsystems, Wetzlar, Germany) was used and sections were stained with toluidine blue for light microscopy (Axiophot 2 microscope, Zeiss, Oberkochen, Germany).

4.8 Laser scanning microscopy

Laser scanning microscopy (LSM) was performed on 10 µm cryosections obtained as described above. Antibodies against CD77 (i.e. Gb3, rat, 1:250, Bio-Rad, cat# MCA579; Hercules, California, USA) and β-(III)-tubulin (chicken, 1:500, Abcam, cat# ab41489, Cambridge, UK) were used for immunoreactions. We used rabbit anti-rat IgM labelled with cyanine 3.18 fluorescent probe (1:50, Amersham; Piscataway, New Jersey, USA) and Alexa Fluor 488 anti-chicken (1:300; Jackson Laboratory; Bar Habor, Maine, USA) as secondary antibodies together with 4',6-diamidino-2-phenylindole (DAPI, 1:10.000; Sigma-Aldrich, cat# 28718-90-3, Taufkirchen, Germany). Photomicrographs were obtained with an inverted IX81 microscope (Olympus, Hamburg, Germany) using an Olympus FV1000 confocal laser scanning system, a FVD10 SPD spectral detector and diode lasers of 405, 473, 559, and 635 nm. All images were acquired with an Olympus UPLSAPO60x objective (oil, numerical aperture: 1.35). A pinhole setting representing one Airy disc was used for high-resolution confocal scanning. High-resolution confocal settings were calibrated to meet an optimum resolution of three pixels per feature in x–y direction. In z-direction, 600 nm steps were used. 12-bit Z-stack images were processed by maximum intensity projection and were adjusted in brightness and contrast using Fiji software (ImageJ 1.50g, Wayne Rasband, National Institute of Health, USA) (Schindelin et al., 2012).

4.9 DRG neuron cell culture

Mouse DRG neurons were dissected and cultivated in culture medium containing 25 ng/ml NGF (2.5S, Alomone Labs, cat# N-240; Jerusalem, Israel) according to the following protocol. Mouse spine was cut and extracted from the body. The spine was dissected longitudinally in half and was placed in a petri dish after removing residual tissue. Both halfs were covered with cold DMEM-gentamicin medium (+4°C) (DMEM F/12, Life Technologies, cat# 10565018; Carlsbad, CA, USA; + 0,05 mg/ml Gentamicin, Sigma-Aaldrich, cat# G1397; Taufkirchen, Germany). Afterwards all DRG available were dissected from the recessus and transferred to a small petri dish

(3 cm) with cold DMEM-gentamicin (+4°C). Residual nerves and tissue were removed and DRG were transferred to another small petri dish (3 cm) with cold DMEM-gentamicin for further processing under the laminar flow and sterile conditions. DRG were then transferred in a 15 ml centrifuge tube (Greiner Bio-one, Kremsmünster, Austria) and DMEM-gentamicin medium was removed. Five ml DMEM medium containing liberase DL (0.28 Wünsch units/ml, Roche, cat# 05466202100; Rotkreuz, Switzerland) was added to digest surrounding tissue for one hour (37°C). Afterwards, DRG were washed two times with 7 ml phosphate buffered saline (PBS, Biochrom, Berlin, Germany). To completely dissolve residual tissue, 5 ml trypsin-EDTA (0.05%, Life Technologies, cat# 25300054; Carlsbad, CA, USA) was added to DRG neurons, followed by another incubation step (15 min, 37°C). After removing trypsin, cell suspension was washed three times with 5 ml DMEM-gentamicin medium at room temperature and once with 5 ml culture medium (100 ml TNB-100, Biochrom, cat# F8023; Berlin, Germany; + 2 ml PenStrep, Life Technologies, cat# 15140-122; Carlsbad, CA, USA; + 100 µl L-glutamine, Life Technologies, cat# 25030-032; Carlsbad, CA, USA; + 2 ml protein-lipid-complex (Biochrom, cat# F8820; Berlin, Germany). Culture medium then was exchanged by 1.5 ml fresh culture medium and ganglia were dissociated with a fire-polished and autoclaved Pasteur pipette resulting in a cell suspension. For centrifugation, 7.5 ml culture medium containing 3.5% BSA (Sigma-Aaldrich, cat# A2058; Taufkirchen, Germany) was filled into a 15 ml centrifuge tube. Cell suspension was then layered on top and centrifuged for 10 minutes at 92 g. This step was repeated to obtain a clean DRG culture. After removing the supernatant, cell pellet was resuspended in 3 ml culture medium and centrifuged for five minutes at 213 g. Cells then were resuspended in 50 µl culture medium per cover slip containing 25 ng/ml mouse NGF. Fifty µl of cell suspension was pipetted to a glass cover slip and incubated for two hours. A final volume of 1 ml culture medium containing 25 ng/ml NGF was added for further cultivation. Cells were cultivated for three to eight days, depending on axonal growth rate. DRG neurons with less than <25 pF resistance were identified as nociceptors and analyzed via patch clamp analysis.

4.10 DRG protein expression

To analyze protein expression, all DRG available were collected (see above) and frozen at -80 °C until further processing. DRG of at least four mice each were pooled

to achieve the recommended tissue weight of ≥300 mg. This was performed three times to obtain three separate replicates. DRG were homogenized using a Polytron PT 3100 homogenizer (Kinematica, Luzern, Switzerland) in 500 µl PBS. The suspension was centrifuged 15 minutes at 1500 g and the supernatant was separated in aliquots à 200 µl. Protein expression levels Mouse Nav1.7 ELISA kit (BlueGene, 0,1ng/ml, cat# E03N0034, Shanghai, China) was used following the manufacturer`s instructions using undiluted samples.

4.11 Patch clamp analysis

Electrophysiological measurements were performed with a TURBO TEC-10 C amplifier (npi, Tamm, Germany). Whole-cell recordings were assessed 3 to 8 days after isolation of DRG neurons at room temperature in a bath solution consisting of 135 mM NaCl, 5.4 mM KCl, 1.8 mM CaCl2, 1 mM MgCl2, 10 mM glucose, and 5 mM HEPES (Hamill et al., 1981). Bath solution for human embryonic kidney 293 (HEK) cells consisted of 140 mM NaCl, 3mM KCl, 1mM CaCl2, 1 mM MgCL2, and 10 mM HEPES. Patch pipettes were pulled from borosilicate glass capillaries (Kimble Chase Life Science and Research Products, Meiningen, Germany) and were heat-polished to reach an input resistance of 2 to 4 MΩ (whole-cell). The pipette recording solution contained 140 mM KCl, 2 mM $MgCl_2$, 1 mM EGTA, 1 mM ATP, and 5 mM HEPES for DRG neuron analysis and 140 mM CsF, 1mM EGTA, 10 mM NaCl, and 10 mM HEPES for HEK cell analysis. Currents were recorded with an EPC9 patch-clamp amplifier (HEKA, Ludwigshafen, Germany) and were low pass-filtered at 1-2 kHz. Stimulation and data acquisition were controlled by the PULSE/PULSEFIT software package (HEKA, Ludwigshafen, Germany) on a Macintosh computer, and data analysis was performed off-line with IGOR software (WaveMetrics, Lake Oswego, OR, USA). Sodium channels were identified using tetrodotoxin (TTX, Alomone Labs, cat# T-550; Jerusalem, Israel). TTX was applied to DRG neurons using a standard perfusion system (Valve commander, Scientific instruments, Gilching, Germany) with a concentration of 100 nM and 1 µM. Cells were first perfused with bath solution, second with TTX solution, and afterwards with bath solution again to observe if sodium currents recover from TTX induced block. During all perfusion steps sodium currents were recorded. Additionally, to quantify TRPV1 currents, 500 nM capsaicin (Merck Millipore, cat# 211275, Darmstadt, Germany) was applied to DRG neurons.

4.12 Short-hairpin (sh) RNA for gene silencing

HEK cells expressing $Na_v1.7$ were received as a kind donation (S. Waxman and S. Dib-Hajj; Center for Neuroscience and Regeneration Research, Yale Medical School and Veterans Affairs Hospital). Cells were cultivated in DMEM F/12 Medium (Life Technologies, cat# 10565018; Carlsbad, CA, USA) containing 10% fetal calf serum (FCS), 1% PenStrep (Life Technologies, cat# 15140-122; Carlsbad, CA, USA), and 0.6 mg/ml Geneticin (G418, Life Technologies cat#10131035; Carlsbad, CA, USA). For knock-down of the α-Gal A gene expression, cells were transfected with short hairpin RNA from the MISSION® shRNA Bacterial TRC2 library (Sigma-Aldrich, Taufkirchen, Germany) or TRC2 pLKO.5-puro non-mammalian shRNA (SHC202) as a control. TRC2-pLKO-puro vector containing shRNA sequence CCGGGATTCGCCAGCTAGCTAATTACTCGAGTAATTAGCTAGCTGGCGAATCTT TTTG (Clone ID:NM_000169.2-458s21c1) was amplified and transfected using lipofectamin 3000 transfection reagent (Life Technologies, cat# L3000008, Carlsbad, CA, USA) into HEK cells. Cells were transfected according to the provided manufacturer`s protocol in a six-well plate using 3.75 µl lipofectamin 3000 and 1.5 µg DNA per well. P3000 reagent was omitted for transfection with si- and shRNAs. Cells were co-transfected with shRNA plasmid and a plasmid expressing green fluorescent protein (GFP). Cells were then incubated in DMEM F/12 medium containing transfection medium for three days. After this period transfection was repeated, to incubate HEK cells for six days in total to knock-down α-Gal A gene expression. Cells transfected with shRNA and those with non-mammalian shRNA as a control were used for patch clamp analysis and immunocytochemistry. Additionally, transfected HEK cells were incubated with 1.32 µl (1mg/ml) agalsidase-alpha 24 hours before patch clamp analysis to investigate, if functional alteration of ion channels can be reversed.

4.13 Immunocytochemistry

After the transfection period, cells were immunoreacted with antibodies against CD77 to investigate Gb3 deposits in HEK cells transfected with shRNA against α-Gal A and non-mamamalian shRNA as a control, as well as cells treated with agalsidase-alpha. Antibodies against CD77 (i.e. Gb3, rat, 1:250, Bio-Rad, cat#; Hercules, CA, USA) were used. Alexa Fluor 488 anti-rat IgM (1:300; Jackson Laboratory, Bar Habor, MA, USA) was applied as secondary antibody together with DAPI (1:10.000; Sigma-

Aldrich, cat# 28718-90-3, Taufkirchen, Germany). Photomicrographs were assessed manually (Axiophot 2 microscope, Zeiss, Oberkochen, Germany) using Spot Advanced Software (Windows Version 5.2). The same exposure time and gain was applied each.

4.14 Statistical analysis

For statistical analysis SPSS IBM software Version 23 (Ehningen, Germany) and for graph design, GraphPad PRISM Version 5.03 (GraphPad Software, Inc., La Jolla, CA, USA) was employed. Data distribution was tested using the Kolmogorov-Smirnov test. The non-parametric Mann-Whitney U test was applied, since data were not normally distributed. Pain behavioral data are expressed as line charts representing the mean and standard error of the mean; all other data are illustrated as box plots, representing the median value and the upper and lower 25% and 75% quartile and as bar graphs representing the mean and the standard error of the mean. Data were stratified for age groups (young: ca. 3 months, old: 12-24 months) and treatment (naïve, CFA i.pl., NaCl, CCI, Sham). P values <0.05 were considered statistically significant.

5. Results

5.1 Old GLA KO mice are protected from mechanical and heat hypersensitivity after i.pl. CFA

Young GLA KO mice displayed increased sensitivity to heat compared to young WT mice at baseline ($p<0.05$, Fig. 3A), while old GLA KO mice were less sensitive to the heat stimuli compared to old WT mice ($p<0.01$, Fig. 3A). Already one hour after CFA injection all mice developed heat hypersensitivity except for old GLA KO mice, which remained on baseline levels during the entire test period of seven days ($p<0.001$, Fig. 3A). Paw withdrawal latencies to cold were elevated in old GLA KO compared to old WT mice at baseline ($p<0.05$, Fig. 3B). There were no differences after i. pl. CFA injection except for old GLA KO mice compared to old WT at day seven ($p<0.05$, Fig. 3B). Young GLA KO and young WT mice had reduced mechanical withdrawal thresholds compared to old GLA KO and old WT mice ($p<0.01$ each, Fig. 3C). One hour after CFA injection all mice showed mechanical hypersensitivity ($p<0.001$, Fig. 3C) which was less pronounced in old GLA KO mice ($p<0.05$, Fig. 3C). Old GLA KO mice were also less sensitive to mechanical stimuli 48 hours after CFA injection compared with old WT mice ($p<0.05$, Fig. 3C), but all mice remained hypersensitive until the end of the test period on day seven. Pain behavior did not differ between genotypes and age-groups after injection of 0.9% NaCl as a control. Results are exemplified for heat withdrawal latencies (Fig. 3D)

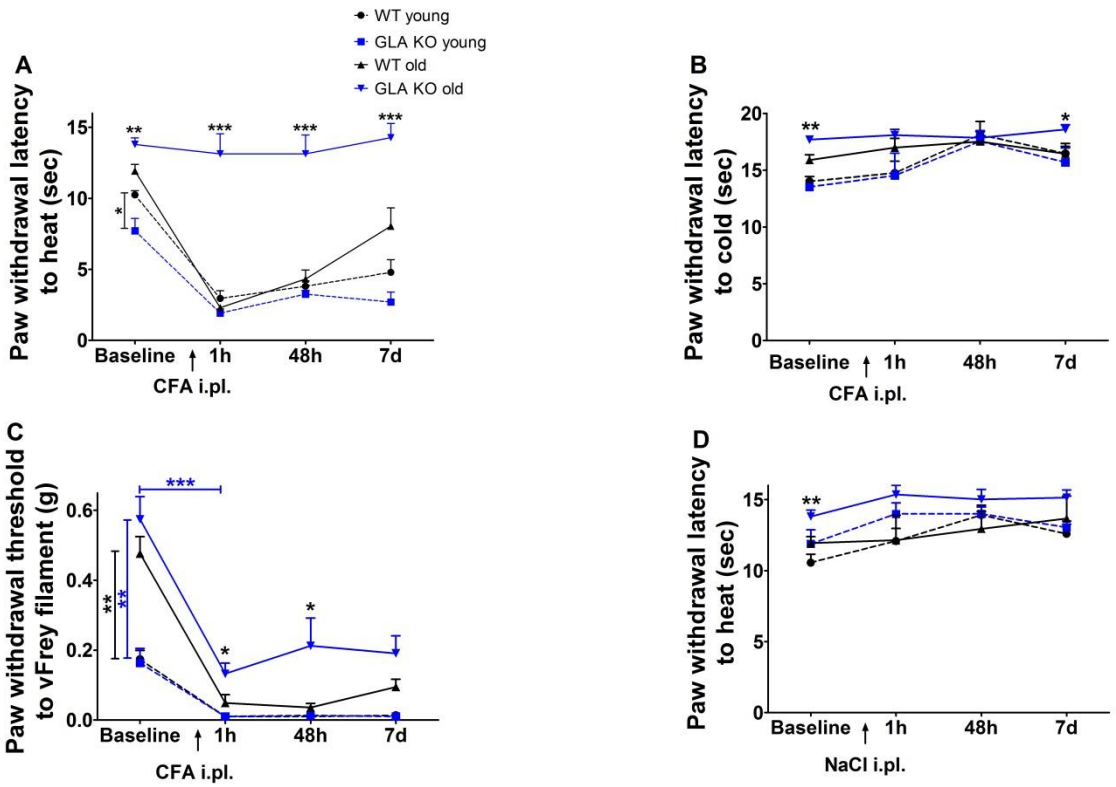

Figure 3: Thermal and mechanical paw withdrawal latencies and thresholds baseline and after i.pl. CFA injection

Line charts show the results of the thermal withdrawal latencies and mechanical withdrawal thresholds in young (3 months) and old (12-24 months) α-GAL deficient (GLA KO) and wildtype littermate (WT) mice. Mice were investigated at baseline, one and 48 hours, and seven days after i.pl. complete Freund`s adjuvant (CFA) injection into the right hind paw. A) Young GLA KO mice were hypersensitive to heat stimulation with shorter heat withdrawal latencies compared to young WT mice ($p<0.05$), while old GLA KO mice showed longer withdrawal latencies to heat compared to old WT mice ($p<0.01$). Already one hour after i.pl. CFA injection, all mice displayed heat hypersensitivity except for old GLA KO mice that showed heat withdrawal latencies similar to baseline for the entire study period of seven days ($p<0.001$). B) Baseline paw withdrawal latencies to cold were longer in old GLA KO mice compared to old WT mice ($p<0.05$). After i.pl. CFA injection no changes were detected for cold sensitivity, except for longer withdrawal latencies in old GLA KO mice compared to old WT mice at day seven ($p<0.05$). C) Young GLA KO and WT mice showed reduced mechanical withdrawal thresholds compared to respective old littermates ($p<0.01$ each). All mice developed mechanical hypersensitivity starting one hour after CFA injection compared to baseline ($p<0.001$), however, old GLA KO mice were less impaired compared to old WT mice ($p<0.05$). While old GLA KO mice were still less sensitive to mechanical stimulation compared to old WT mice 48 h after CFA injection ($p<0.05$), all mice remained mechanically hypersensitive until day seven after CFA i.pl.. There were no changes and differences in pain behavior after injection of 0.9% NaCl as a control, exemplified for heat withdrawal latencies (D).GLA KO: young (3 months; 4 male, 2 female), old (12-24 months; baseline: 12 male, 12 female; CFA: 6 male, 6 female). WT: young (3 months; 4 male, 2 female), (12-24 months; baseline: 12 male, 12 female; CFA: 6 male, 6 female). *$p<0.05$, **$p<0.01$, ***$p<0.001$.

5.2 Old GLA KO mice are protected from mechanical and heat hypersensitivity after CCI

Heat sensitivity of old GLA KO was reduced compared to old WT mice at baseline ($p<0.01$, Fig. 4A). Three days after CCI, old WT mice developed heat hypersensitivity ($p<0.01$, Fig. 4A), which was still present at day 28 ($p<0.01$, Fig. 4A), while old GLA KO mice remained at baseline levels during the entire test period of 28 days. Sensitivity to cold stimuli of old GLA KO mice was reduced at baseline compared to old WT mice ($p<0.01$, Fig. 4B), but there was no difference after CCI between both genotypes. There was also no difference between genotypes in mechanical withdrawal thresholds at baseline. Old GLA KO mice remained at baseline levels during the entire test period of 28 days after CCI surgery. In contrast, old WT mice showed increased mechanical sensitivity on day three and seven ($p<0.01$, Fig. 4C) up to day 28 ($p<0.01$, Fig 4C). Pain behavior did not differ between genotypes after sham surgery. Results are exemplified for heat withdrawal latencies (Fig. 4D).

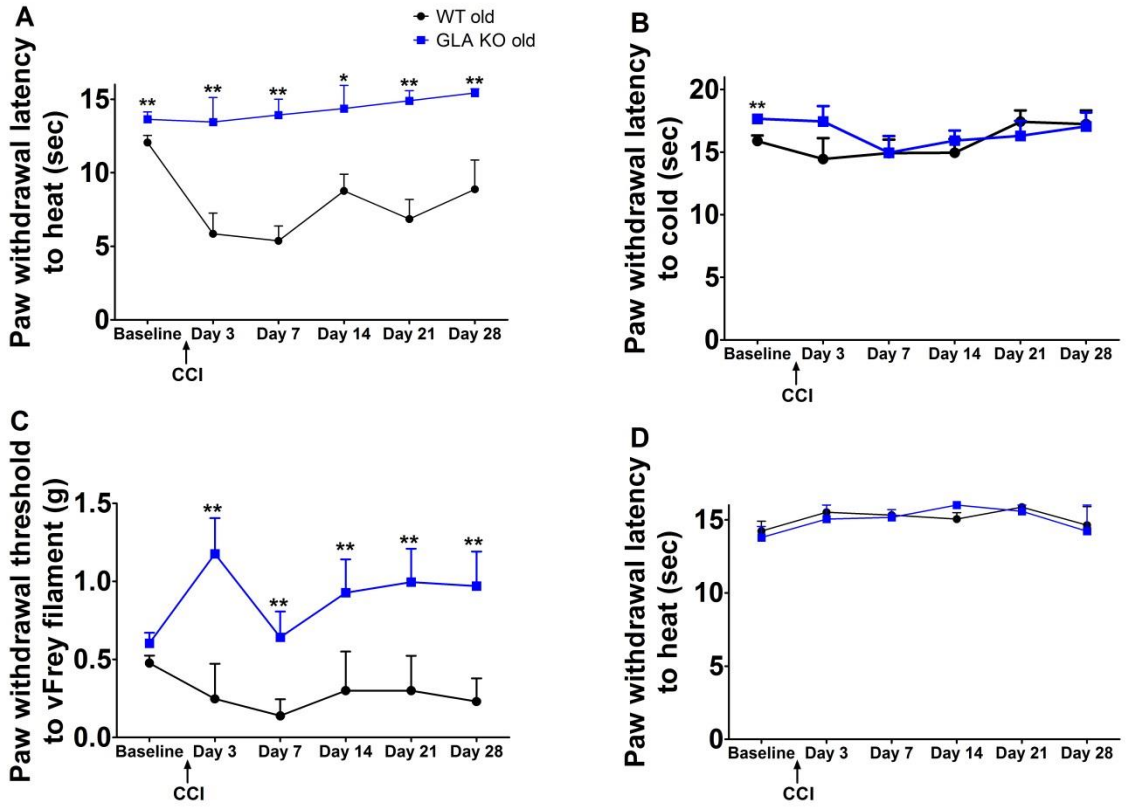

Figure 4: Thermal and mechanical paw withdrawal latencies and thresholds baseline and after CCI

Bar graphs show the results of the thermal withdrawal latencies and mechanical withdrawal thresholds in old (12-24 months) α-GAL deficient (GLA KO) and wildtype littermate (WT) mice. Mice were

investigated at baseline, three, seven, 14, 21, and 28 days after chronic constriction injury (CCI) of the right sciatic nerve. A) CCI induced heat hypersensitivity only in old WT mice, while old GLA KO mice were spared ($p<0.01$). Hypersensitivity was present from day three up to day 28 after surgery ($p<0.01$), while cold perception latencies (B) did not differ after CCI between both genotypes. C) Old GLA KO mice remained on mechanical withdrawal thresholds similar to baseline for the entire study period of 28 days, while old WT mice displayed hypersensitivity to mechanical stimuli already on day three after CCI ($p<0.01$) until day 28 ($p<0.01$). There were no changes and differences in pain behavior after sham surgery (D). GLA KO: old (12-24 months; baseline: 12 male, 12 female; CCI: 3 male, 3 female). WT: old (12-24 months; baseline: 12 male, 12 female; CCI: 3 male, 3 female). *$p<0.05$, **$p<0.01$.

5.3 I.pl. CFA injection induces anxiety-like behavior in the EPM in GLA KO and WT mice

Time spent in the open arms of the EPM was not different between naïve genotypes and age-groups, except for young WT mice compared to young GLA KO mice ($p<0.05$; Fig. 5A). I.pl. CFA injection led to a decrease in time spent in the open arms in young GLA KO mice compared to young naïve GLA KO mice ($p<0.05$; Fig. 5A). After CFA injection time spent in open arms was also shorter in young GLA KO mice than in young WT mice ($p<0.05$; Fig. 5A). In old mice, CFA i.pl. reduced time spent in open arms in GLA KO ($p<0.01$; Fig. 5A) and in WT mice ($p<0.05$; Fig 5A). There was no intergroup difference in the number of entries into the open arms in naïve and CFA treated mice except for old CFA treated GLA KO mice, which entered less often than old naïve GLA KO mice ($p<0.05$; Fig. 5B). No difference was found in young age-groups for time spent in closed arms. Old CFA treated mice of both genotypes spent more time in the closed arms compared to old naive mice (GLA KO: $p<0.01$; WT: $p<0.001$; Fig. 5C). There was no difference in entries into the closed arms between age-groups and genotypes in the naïve state. After CFA injection young GLA KO mice more often entered the closed arms than young WT mice ($p<0.05$; Fig. 5D). Also, old CFA treated GLA KO mice had more entries into the closed arm than old naïve mice ($p<0.05$; Fig. 5D).

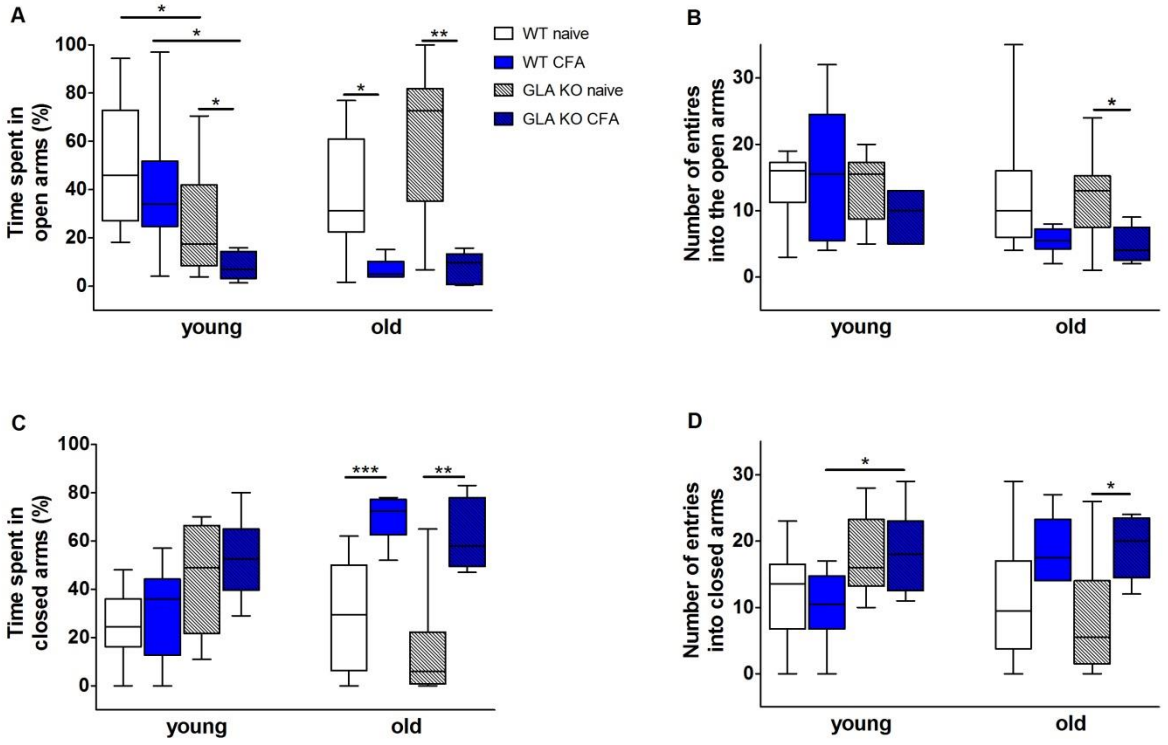

Figure 5: Anxiety-like behavior in the elevated plus maze test.

Boxplots show the results of anxiety-like behavior in the elevated plus maze test (EPM). Young (3 months) and old (12-24 months) α-GAL A deficient (GLA KO) and wildtype littermate (WT) male mice were investigated in the naïve state and after i.pl. complete Freund`s adjuvant (CFA) injection into the right hind paw. A) In the EPM no genotype- or age-associated differences were found for time spent in the open arms and entries into the open arms when comparing naïve mice (A, B), except for longer time spent in open arms by young WT mice compared to young GLA KO mice ($p<0.05$). I.pl. CFA injection reduced time spent in the open arms compared to baseline in young (GLA KO: $p<0.05$; WT: n.s.) and old mice (GLA KO: $p<0.01$; WT: $p<0.05$). The reduction was particularly visible in young GLA KO mice compared to young WT mice ($p<0.05$). B) CFA injection also reduced the number of entries into the open arms in old GLA KO mice ($p<0.05$). C) Young and old age-groups showed no intergroup difference in time spent in closed arms. I.pl. CFA injection induced an increase in time spent in closed arms only in old mice of both genotypes (GLA KO: $p<0.01$; WT: $p<0.001$). D) CFA injection also increased the number of entries into the closed arms in young GLA KO mice compared to young treated WT mice ($p<0.05$) and old GLA KO mice compared to baseline ($p<0.05$). GLA KO: young (3 months; naïve: 10 male; CFA: 6 male), old (12-24 months; naïve: 10 male; CFA: 6 male). WT: young (3 months; naïve: 10 male; CFA: 6 male), old (12-24 months; naïve: 10 male; CFA: 6 male). *$p<0.05$, **$p<0.01$, ***$p<0.001$.

There was no intergroup difference between genotypes, age-groups, and treatment for the time spent in the light box, entries into the light box, time spent in the dark box, and entries into the dark box except for young naïve WT mice compared with young CFA treated WT mice ($p<0.05$ each; Fig. 6).

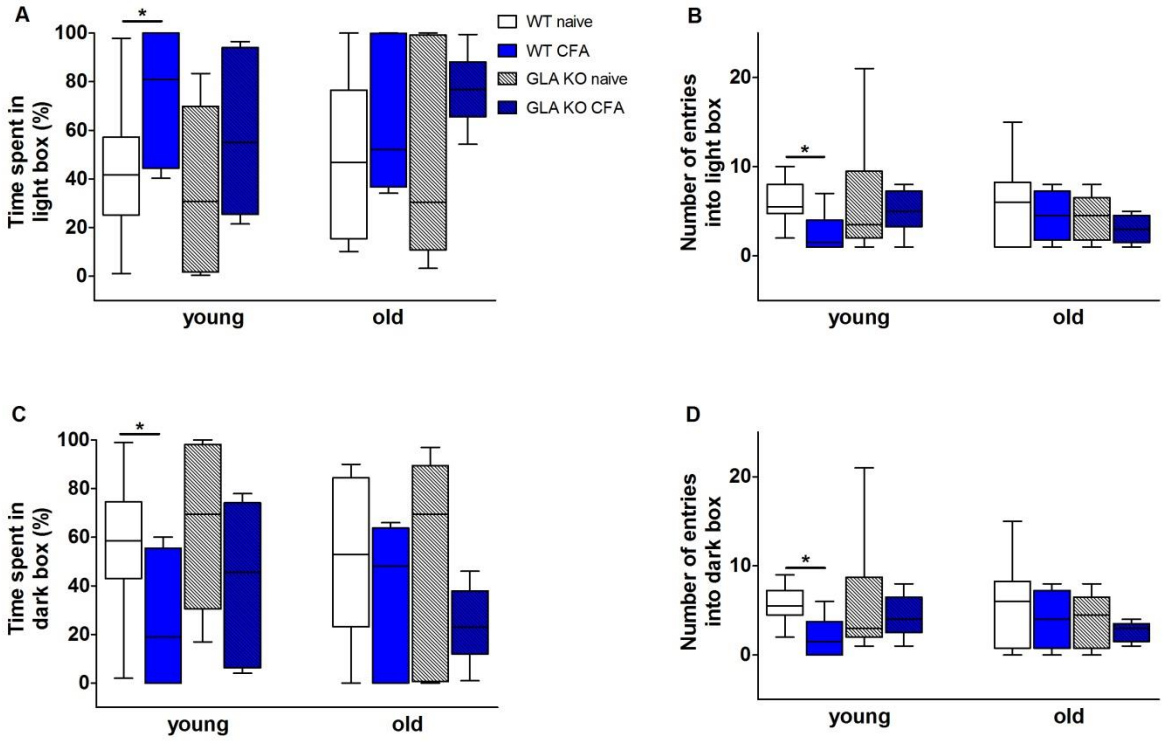

Figure 6: Anxiety-like behavior in the light-dark box test.

Boxplots show the results of anxiety-like behavior in the light-dark box test (LDB). Young (3 months) and old (12-24 months) old α-GAL A deficient (GLA KO) and wildtype littermate (WT) male mice were investigated in the naïve state and after i.pl. complete Freund`s adjuvant (CFA) injection into the right hind paw. In the LDB experiment time spent in the light box (A) and the number of entries into the light box (B), as well as time spent in the dark box (C) and number of entries into the dark box (D) did not differ between genotypes, age- and treatment groups, except for young WT mice in the naïve state compared to CFA treated young WT mice ($p<0.05$ each). GLA KO: young (3 months; naïve: 10 male; CFA: 6 male), old (12-24 months; naïve: 10 male; CFA: 6 male). WT: young (3 months; naïve: 10 male; CFA: 6 male), old (12-24 months; naïve: 10 male; CFA: 6 male). *$p<0.05$.

No difference was found between genotypes, age- and treatment groups in time spent in the center zone, except for young WT mice compared to young GLA KO mice in the naïve state ($p<0.05$; Fig. 7A). Total distance travelled was not different between genotypes, age- and treatment groups except for young GLA KO mice in the naïve state compared with old GLA KO mice ($p<0.01$; Fig. 7B).

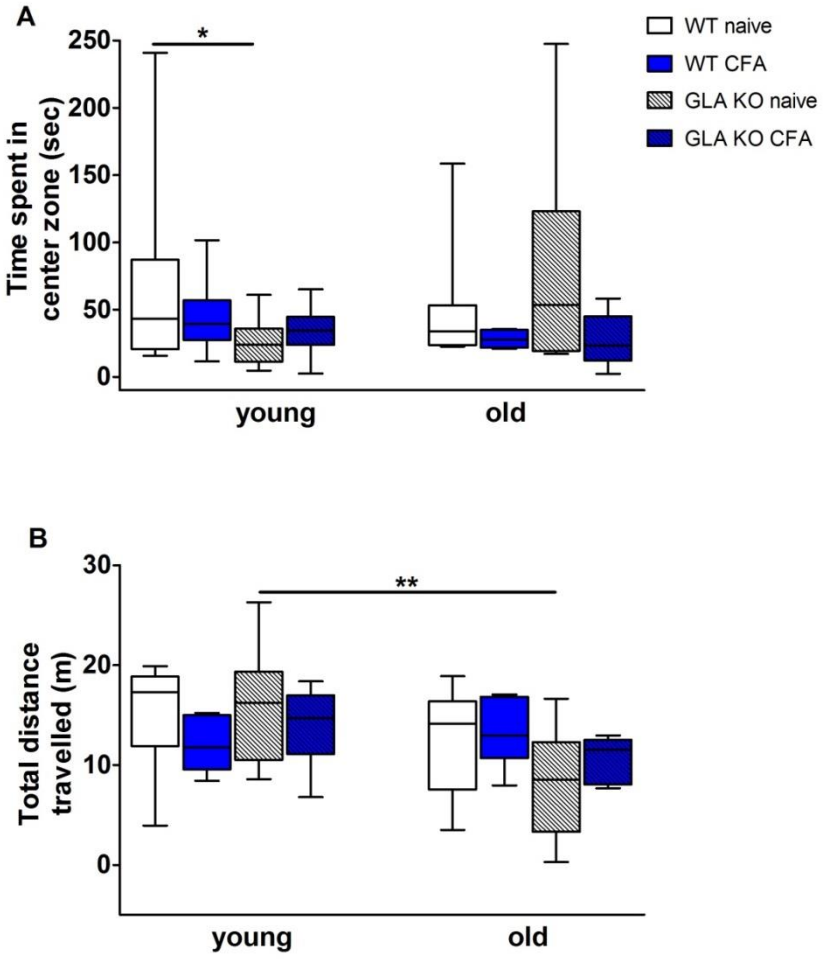

Figure 7: Anxiety-like behavior in the open field test.

Boxplots show the results of the anxiety-like behavior in the open field test (OF). Young (3 months) and old (12-24 months) old α-GAL A deficient (GLA KO) and wildtype littermate (WT) mice were investigated in the naïve state and after i.pl. complete Freund`s adjuvant (CFA) injection into the right hind paw. (A) Time spent in the central central zone of the OF only differed between young WT and young GLA KO mice in the naïve state ($p<0.05$). B) Total distances travelled in the OF were longer for naïve young GLA KO mice compared to old GLA KO mice ($p<0.01$). GLA KO: young (3 months; naïve: 10 male; CFA: 6 male), old (12-24 months; naïve: 10 male, CFA: 6 male). WT: young (3 months; naïve: 10 male; CFA: 6 male), old (12-24 months; naïve: 10 male; CFA: 6 male). *$p<0.05$, **$p<0.01$.

5.4 No depression-like behavior in GLA KO mice

There was no intergroup difference in the assessment of potential depression-like behavior in the FST. Naïve GLA KO and WT mice spent similar time spans immobile in the water basin (GLA KO: median 180.8 sec, range 160.6-221.4 sec; WT: median 154.6 sec, range 127.6-225.7 sec; Fig. 8).

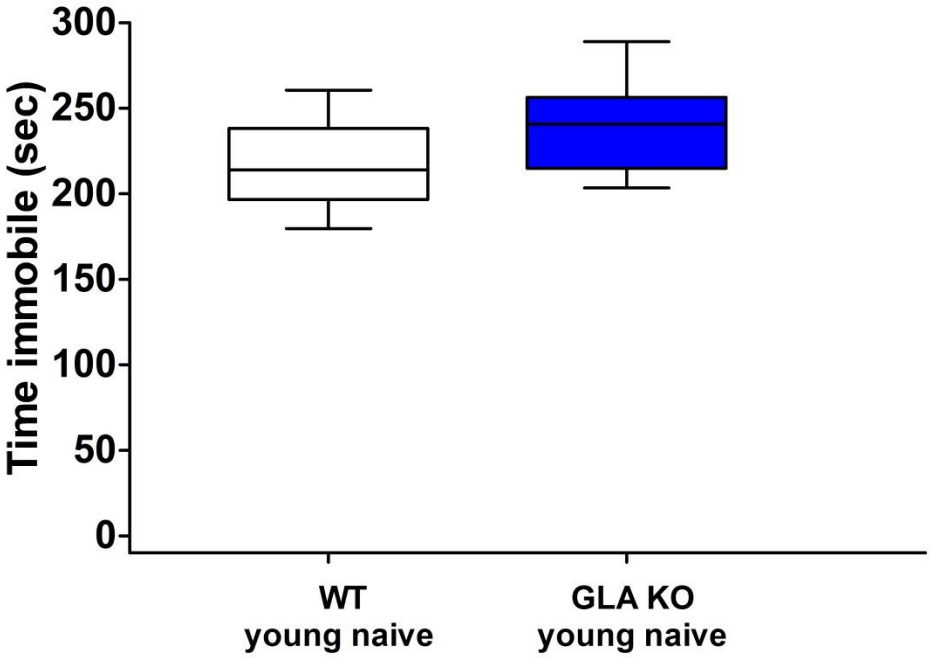

Figure 8: Depression-like behavior in the forced swim test.
Boxplots show the results for depression-like behavior in the forced swim test (FST). Young naive (3 month) α-GAL A deficient (GLA KO) and wildtype (WT) male mice were investigated. There was no difference between the genotypes. GLA KO: young (3 months; 10 male). WT: young (3 months; 10 male).

5.5 Similar learning behavior in GLA KO and WT mice

In the training session, test duration displayed no relevant differences between genotypes and age-groups and continuously decreased from training day one to four (Fig. 9).

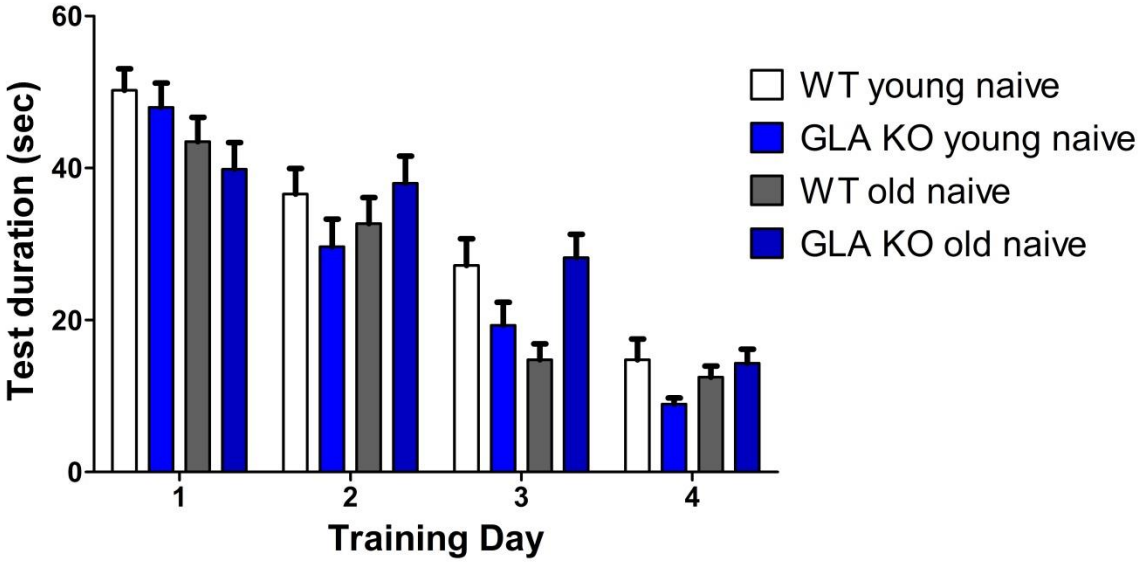

Figure 9: Learning behavior in the Morris water maze test.

Bar graphs show the results of the learning behavior in the Morris water maze test (MWM). Naive young (3 months) and old (12-24 months) α-GAL deficient (GLA KO) and wildtype littermate (WT) male mice were investigated. No relevant differences were found in mice of both genotypes and age-groups for total test duration; time spent until finding the hidden platform continuously decreased from training day one to four. GLA KO: young (3 months; 10 male), old (12-24 months; 10 male). WT: young (3 months; 10 male), old (12-24 months; 10 male).

In the probe trial, time travelled in the target quadrant did not differ between genotypes and age-groups (Fig. 10A). Latency until first entry into the target zone was shorter for mice of the young age-group compared to old mice, as expected (GLA KO: $p<0.01$; WT: $p<0.05$; Fig 10B).

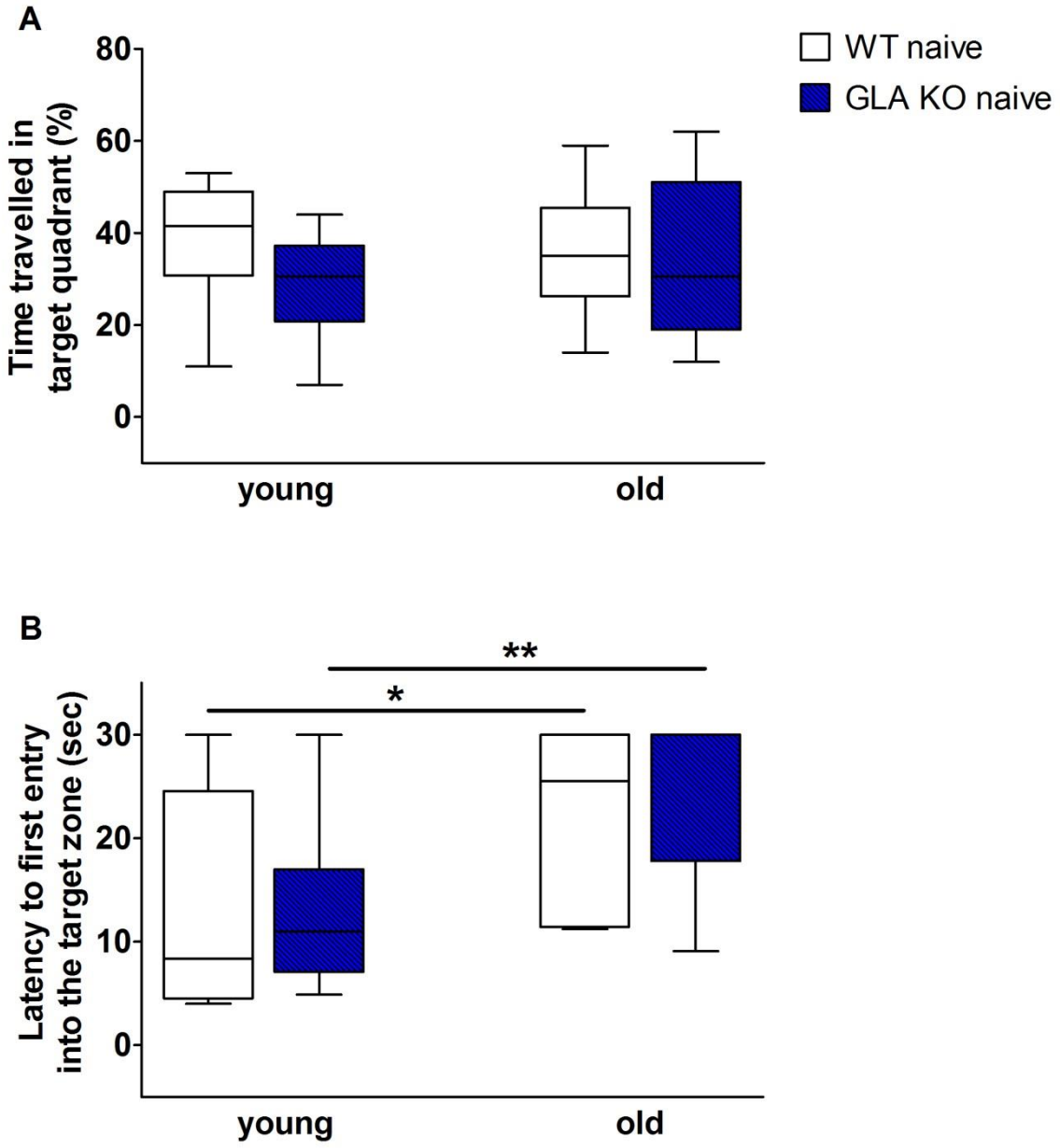

Figure 10: Memory function in the Morris water maze test.

Boxplots show the results of memory function in the Morris water maze test (MWM). Naive young (3 months) and old (12-24 months) old α-GAL A deficient (GLA KO) and wildtype littermate (WT) male mice were investigated. In the probe trial, time travelled in the target quadrant was not different between genotypes and age-groups (A). As expected, the latency until first entry into the target zone was shorter for young compared to old mice of both genotypes (GLA KO: $p<0.01$; WT: $p<0.05$; B). GLA KO: young (3 months; 10 male), old (12-24 months; 10 male). WT: young (3 months; 10 male), old (12-24 months; 10 male). *$p<0.05$, **$p<0.01$.

5.6 No differences in gene expression of pain related neuronal ion channels between genotypes, age- and treatment groups

There was no difference in gene expression of pain related ion channels in DRG, except for young WT mice in the naïve state compared to CFA treated young WT mice, which displayed lower gene expression of HCN2 channel seven days after intervention ($p<0.05$; Fig 11 B).

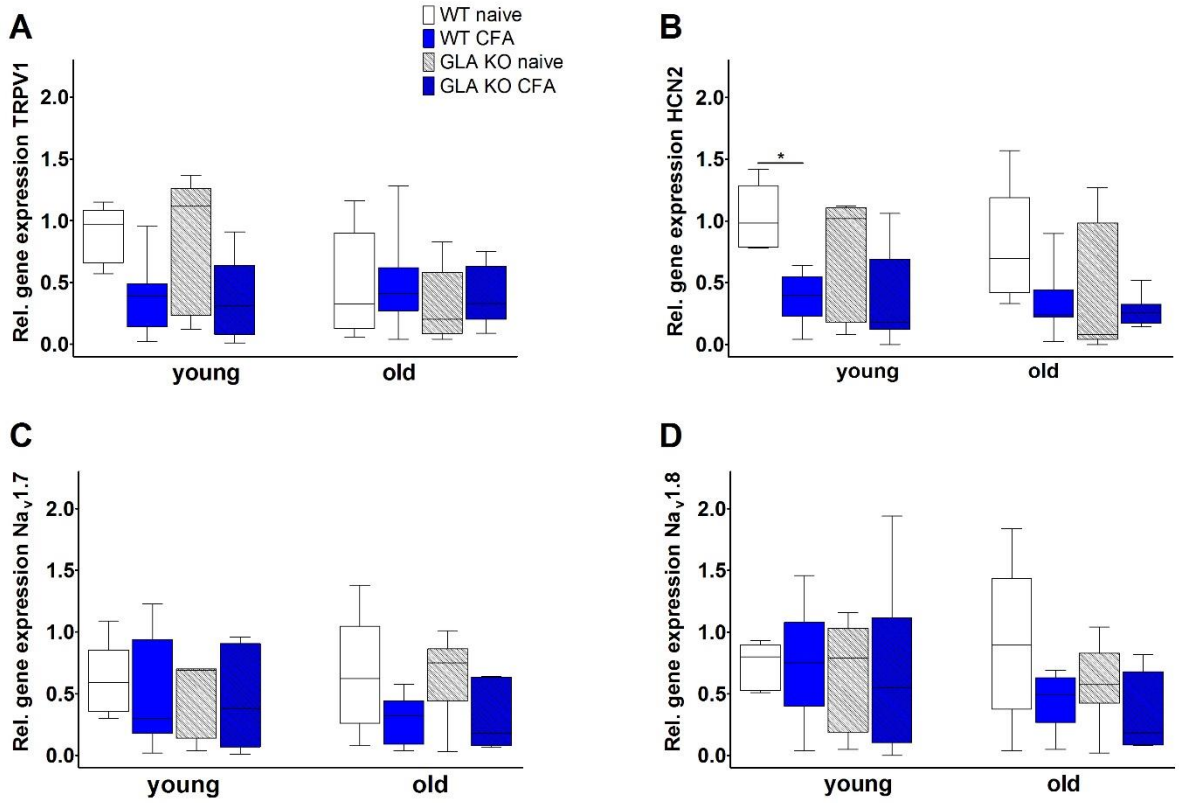

Figure 11: Gene expression of pain related ion channels in DRG at basline and after i.pl. CFA injection

Boxplots show the results of ion channel gene expression in dorsal root ganglia (DRG) of young (3 months) and old (12-24 months) α-GAL deficient (GLA KO) and wildtype littermate (WT) mice before and seven days after i.pl. complete Freund`s adjuvant (CFA) injection. DRG gene expression of transient receptor potential vanilloid 1 (TRPV1; A), potassium/sodium hyperpolarization-activated cyclic nucleotide-gated ion channel 2 (HCN2; B), voltage-gated sodium channel 1.7 ($Na_v1.7$; C), and voltage-gated sodium channel 1.8 ($Na_v1.8$; D) did not differ between genotypes, age- and treatment groups, except young WT mice in the naïve state compared to young CFA treated WT mice displayed higher expression of HCN2 channel ($p<0.05$). GLA KO: young (3 months; naïve: 5 male; CFA: 7 male), old (12-24 months; naïve: 12 male; CFA: 6 male). WT: young (3 months; naïve: 7 male; CFA: 6 male), old (12-24 months; naïve: 12 male; CFA: 6 male). *$p<0.05$.

5.7 Immunoreactivity of neuronal pain related ion channels differs between genotypes and age-groups in naïve mice

There was no difference in immunoreactivity against TRPV1 channels between genotypes and age-groups (Fig.12 A-D). Quantification of TRPV1 positive neurons did not differ between young and old mice of both genotypes, except for old GLA KO mice compared to young GLA KO and old WT mice ($p<0.001$; Fig. 12E).

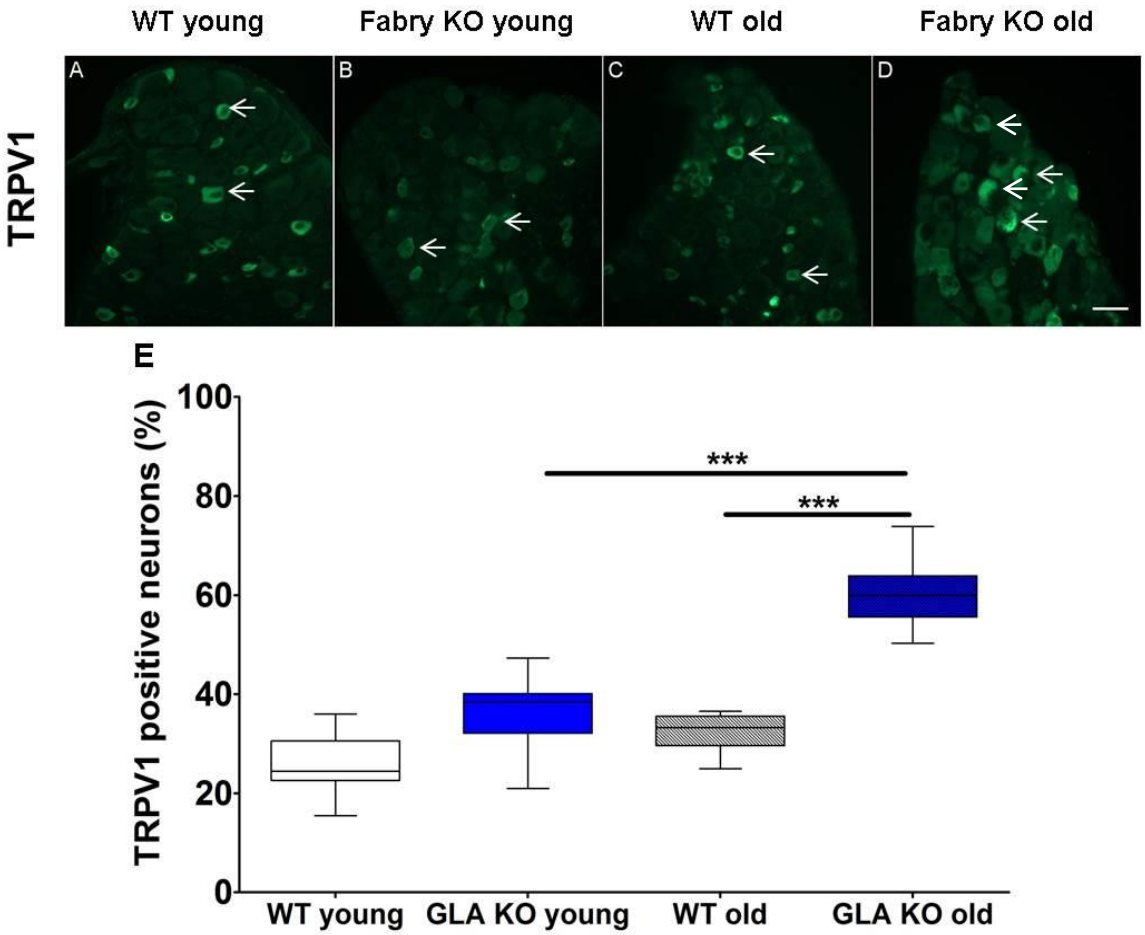

Figure 12: TRPV1 protein expression in DRG neurons

Photomicrographs show immunoreactivity of antibodies against transient receptor potential vanilloid 1 (TRPV1) channels (A-D) in 10 µm cryosections of DRG from young (3 months) and old (12-24 months) α-GAL deficient (GLA KO) and wildtype littermate (WT) mice. Boxplots (E) show quantifictaion of TRPV1 channel positive neurons. TRPV1 immunoreactivity in the DRG was not different between genotypes and age-groups (A-D), however, quantification of TRPV1 channel positive neurons was higher in old GLA KO mice compared to young GLA KO mice ($p<0.001$; E) and old WT mice ($p<0.001$; E). Scale bar: 50 µm. GLA KO: young (3 months: 6 mice), old (12-24 months: 6 mice). WT: young (3 months: 6 mice), old (12-24 months: 6 mice). ***$p<0.001$. Arrows point to immune-positive neurons. This experiment was performed by Dorothea Hose.

Immunoreactivity to HCN2 did not differ between genotypes in the young age-group (Fig. 13A, B, E). It also was not differ between genotypes in the old age-group (Fig. 13C, D, E), but was lower in the young compared with the old age-group ($p<0.05$; Fig. 13E).

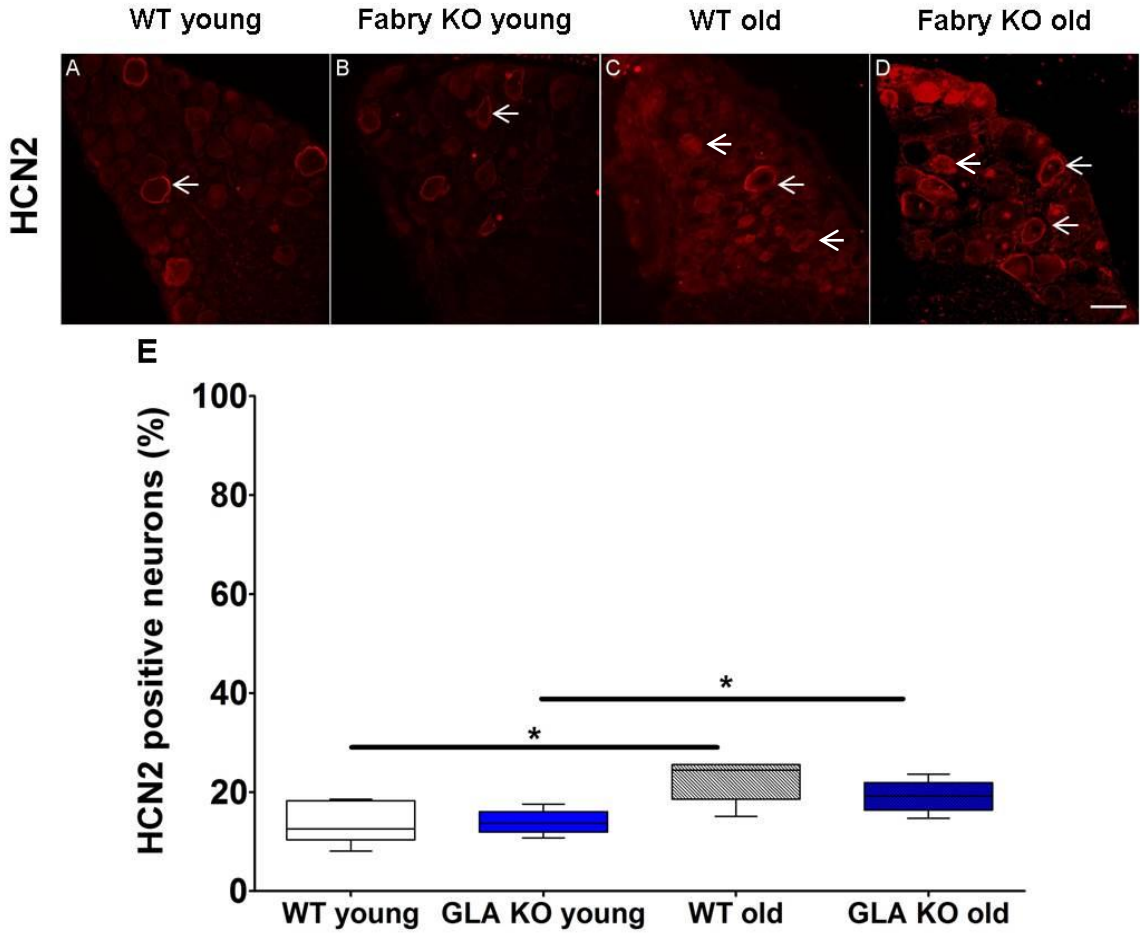

Figure 13: HCN2 protein expression in DRG neurons

Photomicrographs show immunoreactivity of antibodies against potassium/sodium hyperpolarization-activated cyclic nucleotide-gated ion channel 2 (HCN2) channel (A-D) in 10 µm sections of DRG from young (3 months) and old (12-24 months) α-GAL deficient (GLA KO) and wildtype littermate (WT) mice. Boxplots (E) show quantifictaion of HCN2 channel positive neurons. A-D) Immunoreactivity against HCN2 channel did not differ between genotypes and age-groups. Quantification of HCN2 channel positive neurons was also not different between genotypes, but was lower in the young compared to the old age-group ($p<0.05$) (E). Scale bar: 50 µm. GLA KO: young (3 months: 6 mice), old (12-24 months: 6 mice). WT: young (3 months: 6 mice), old (12-24 months: 6 mice).*$p<0.05$. Arrows point to immune-positive neurons.

$Na_v1.8$ immunoreactivity in DRG neurons revealed no intergroup differences (Fig. 14).

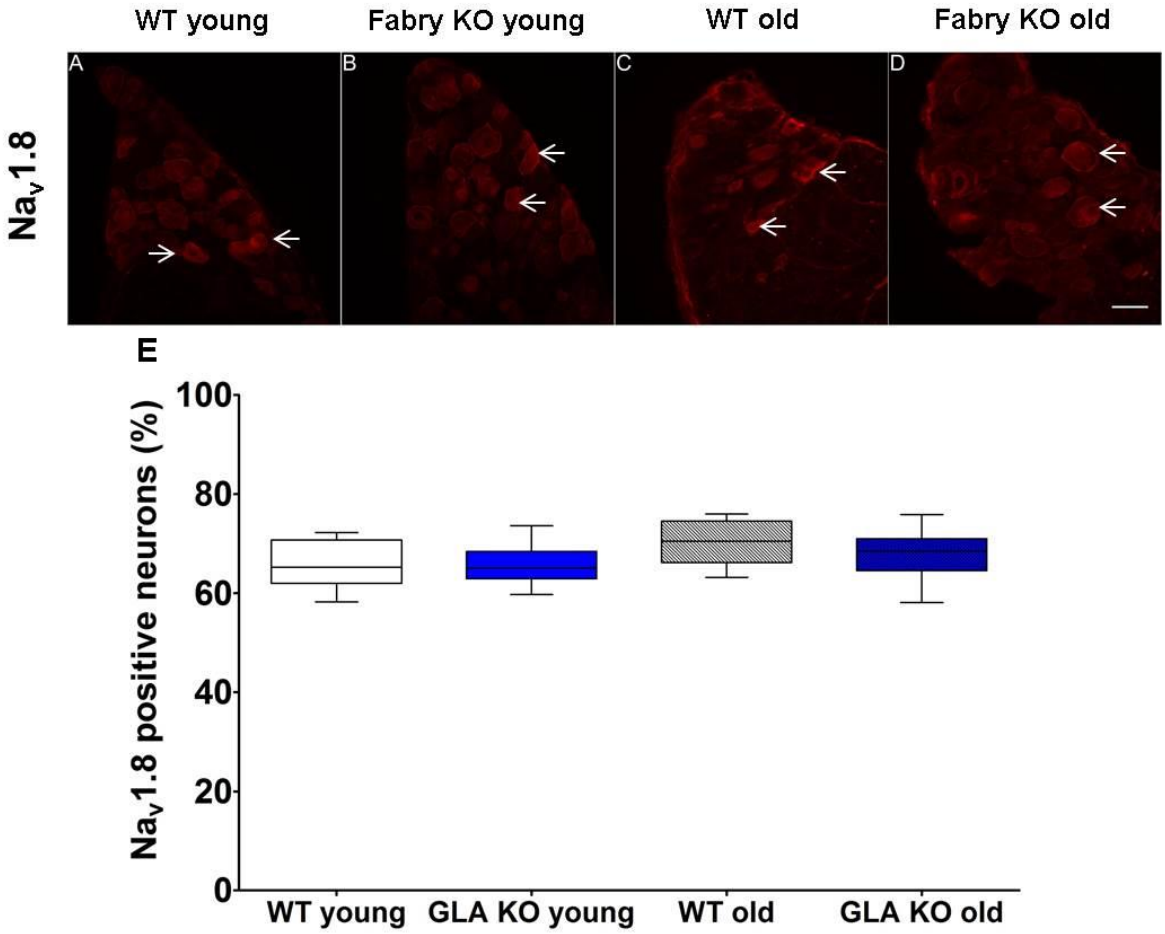

Figure 14: $Na_v1.8$ protein expression in DRG neurons

Photomicrographs show immunoreactivity of antibodies against voltage-gated sodium channel 1.8 ($Na_v1.8$) (A-D) in 10 µm sections of DRG from young (3 months) and old (12-24 months) α-GAL deficient (GLA KO) and wildtype littermate (WT) mice. Boxplots (E) show quantification of sodium channel $Na_v1.8$ positive neurons. A-D) Immunoreactivity against sodium channel $Na_v1.8$ was not different between genotypes and age-groups. Quantification of sodium channel $Na_v1.8$ positive neurons did also not differ between genotypes and age-groups (E). Scale bar: 50 µm. GLA KO: young (3 months: 6 mice), old (12-24 months: 6 mice). WT: young (3 months: 6 mice), old (12-24 months: 6 mice). Arrows point to immune-positive neurons. Young age-groups were investigated by Dorothea Hose.

Since $Na_v1.7$ immunostaining failed using five different types of $Na_v1.7$ antibodies detailed above, we applied ELISA and found no difference of DRG $Na_v1.7$ protein in DRG of all genotypes and age-groups (Fig. 15).

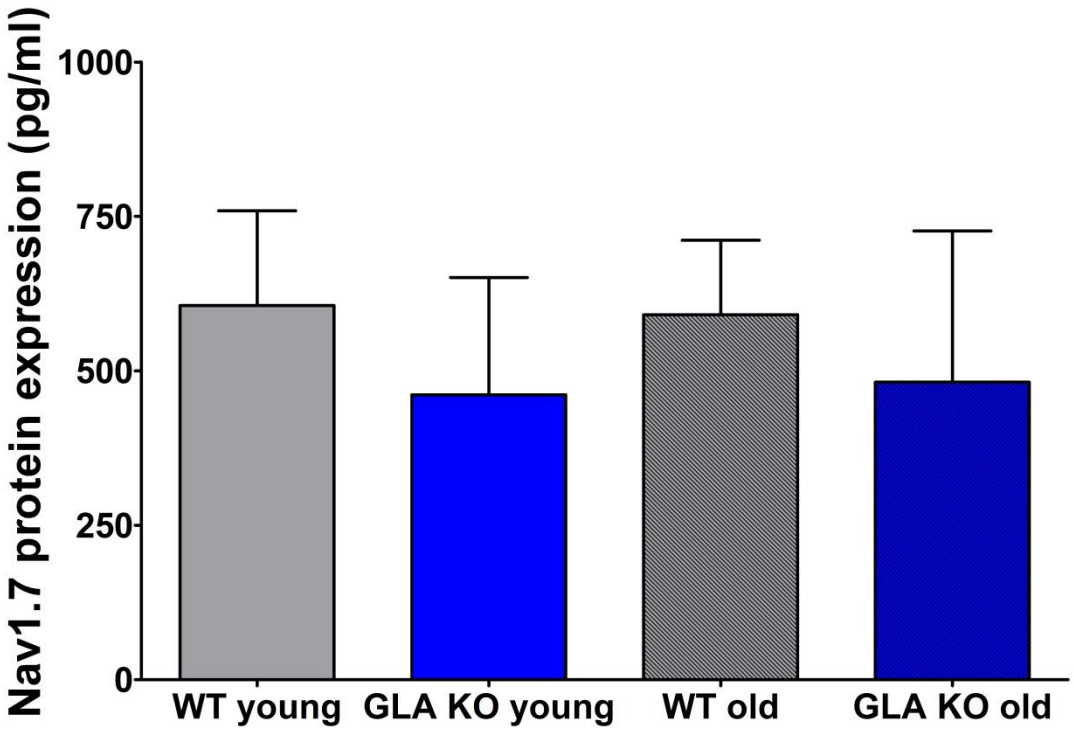

Figure 15: $Na_v1.7$protein expression in DRG

Bar graphs show the results of $Na_v1.7$ protein expression in DRG of young (3 months) and old (12-24 months) α-GAL deficient (GLA KO) and wildtype littermate (WT) mice. There was no difference in $Na_v1.7$ protein expression between genotypes and age-groups. GLA KO: young (3 months: 16 mice), old (12-24 months: 16 mice). WT: young (3 months: 16 mice), old (12-24 months: 16 mice).

5.8 Elevated Gb3 accumulation in DRG neurons of old GLA KO mice

Semithin sections stained with toluidine blue displayed no Gb3 accumulations in DRG neurons of old WT mice, but a high Gb3 load in old GLA KO mice (Fig. 16A-C). Immunoreactivity against CD77 as a marker for Gb3 did not reveal any relevant Gb3 deposits in DRG neurons of young GLA KO, young WT, and old WT mice (Fig. 16D-F). Old GLA KO mice, however, showed abundant Gb3 deposition in many DRG neurons (Fig. 16G).

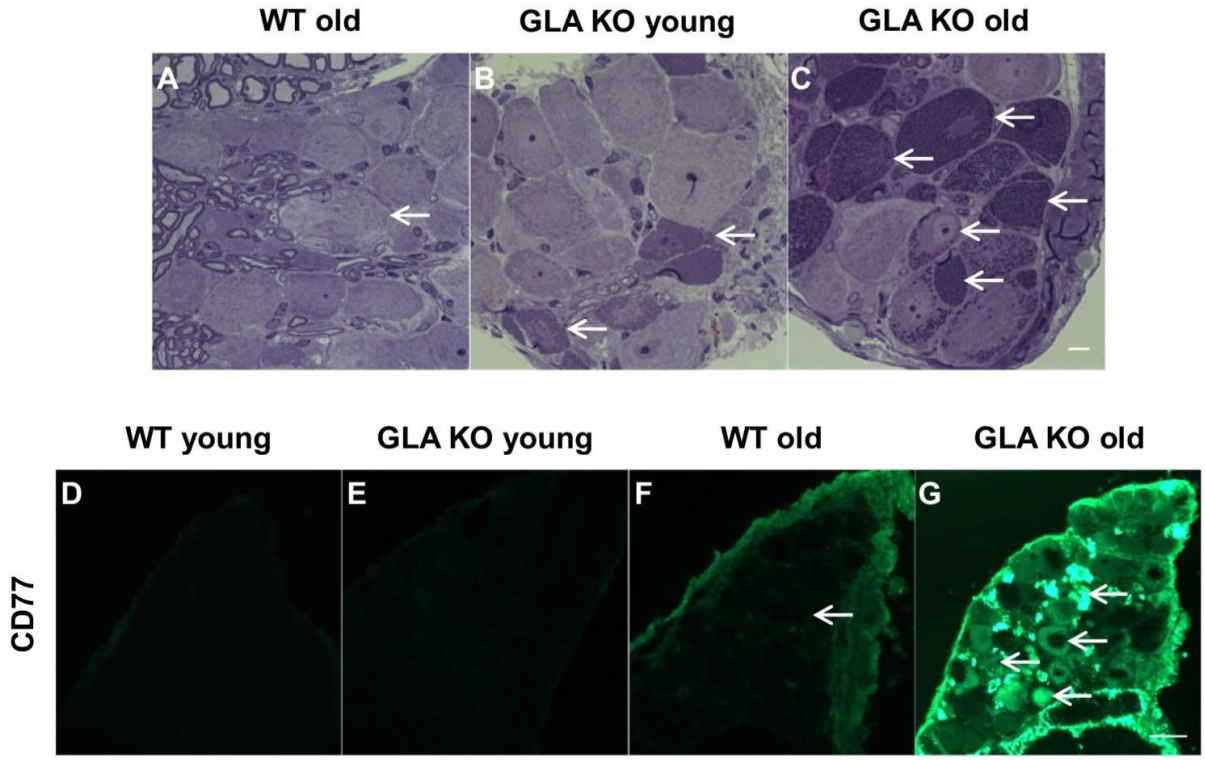

Figure 16: Immunoreaction against CD77 and toluidine blue staining of tissue sections from mouse DRG

Photomicrographs show toluidine blue staining (A-C) of 0.5 µm semithin sections of dorsal root ganglia (DRG) from an old wildtype (WT), a young (3 months) and an old (12-24 months) α-GAL deficient (GLA KO) mouse and immunoreactivity of antibodies against CD77 as a marker for Gb3 (D-G) from young (3 months) and old (12-24 months) α-GAL deficient and WT mice. No depositions were found in DRG neurons of the old WT mouse (A, arrow), neurons of a young GLA KO mouse showed few Gb3 deposits (B, arrows). Old GLA KO mouse, however, displayed elevated Gb3 load in DRG neurons (C, arrows). Additionally immunoreactivity against CD77 was not different in young GLA KO, young WT and old WT mice (D-F), while old GLA KO mice showed increased Gb3 accumulations in DRG neurons (G, arrows). Scale bar semithin: 10µm. Scale bar immunoflurescence: 50µm. Arrows point to stained and immune-positive neurons.

5.9 Gb3 and β-(III)-tubulin are co-localized in the cytoplasm of DRG neurons

Immunoreactivity against CD77 as a marker for Gb3 and β-(III)-tubulin as a cytoplasmic marker revealed that Gb3 accumulates mostly within the cytoplasm of DRG neurons, but potentially also in the cell membrane and descending axons (Fig. 17).

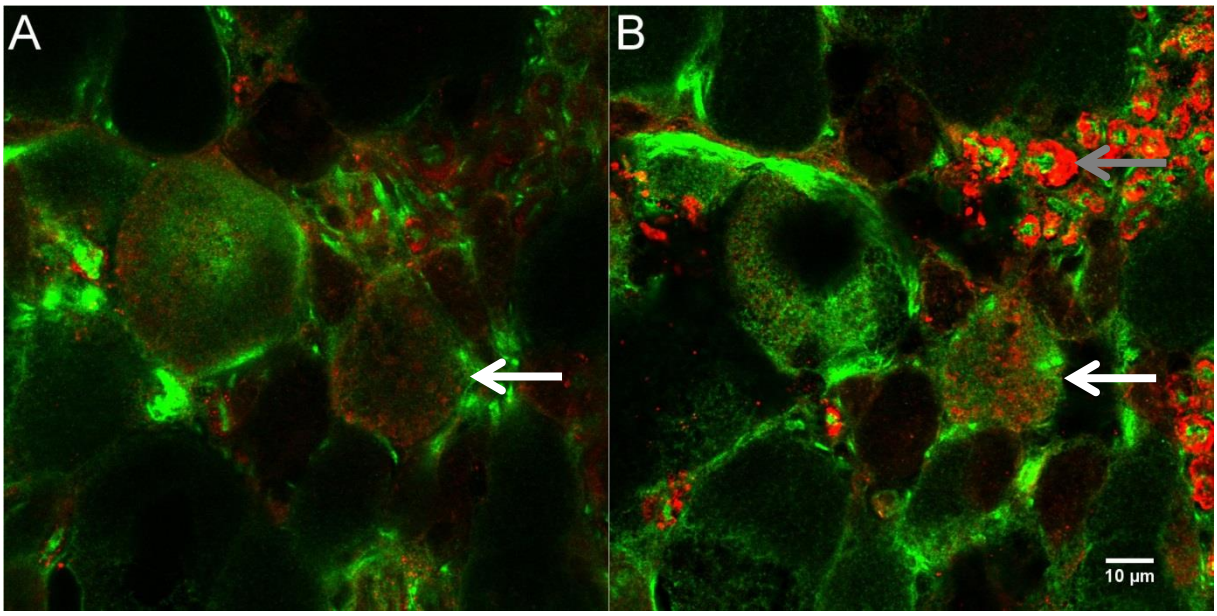

Figure 17: Laser scanning microscopy after immunoreaction of DRG neurons with antibodies against CD77 and β-(III)-tubulin

Photomicrographs show immunoreactivity of antibodies against CD77 as a marker for Gb3 (red) and β-(III)-tubulin as a cytoplasmic marker (green) in dorsal root ganglion (DRG) neurons of an old (20 months) α-GAL deficient (GLA KO) mouse. Co-localization of CD77 and β-(III)-tubulin is displayed from the equator of the cell (A, white arrow) to its top (B, white arrow) providing evidence for intra-neuronal and potentially accumulation of Gb3 in the membrane of the cells and their descending axons (B, grey arrow). Arrows point to an immune-positive neuron (A, B white arrow) and axon (B, grey arrow). Scale bar 10 µm.

5.10 Old GLA KO mice display reduction of DRG neuron sodium and I_h currents

To characterize sodium and I_h currents, maximum potentials of sodium currents and potentials at -120mV for I_h currents were normalized to cell size to calculate current densities. DRG neurons from young GLA KO mice had normal sodium current intensities with fast inactivating kinetics at baseline (Fig. 18A). These sodium currents were sensitive to TTX already at a concentration of 100 nM (Fig. 18B) and recovered completely after washout with bath solution (Fig. 18C). Based on kinetics and TTX sensitivity of sodium currents, we identified the responsible sodium channel as $Na_v1.7$. The most striking finding was that while no differences were seen in sodium current amplitudes between young GLA KO and young and old WT mice, sodium currents were markedly reduced in old GLA KO mice (exemplified current Fig. 18D) comparing with young GLA KO ($p<0.01$) and old WT mice ($p<0.001$; Fig. 18E).

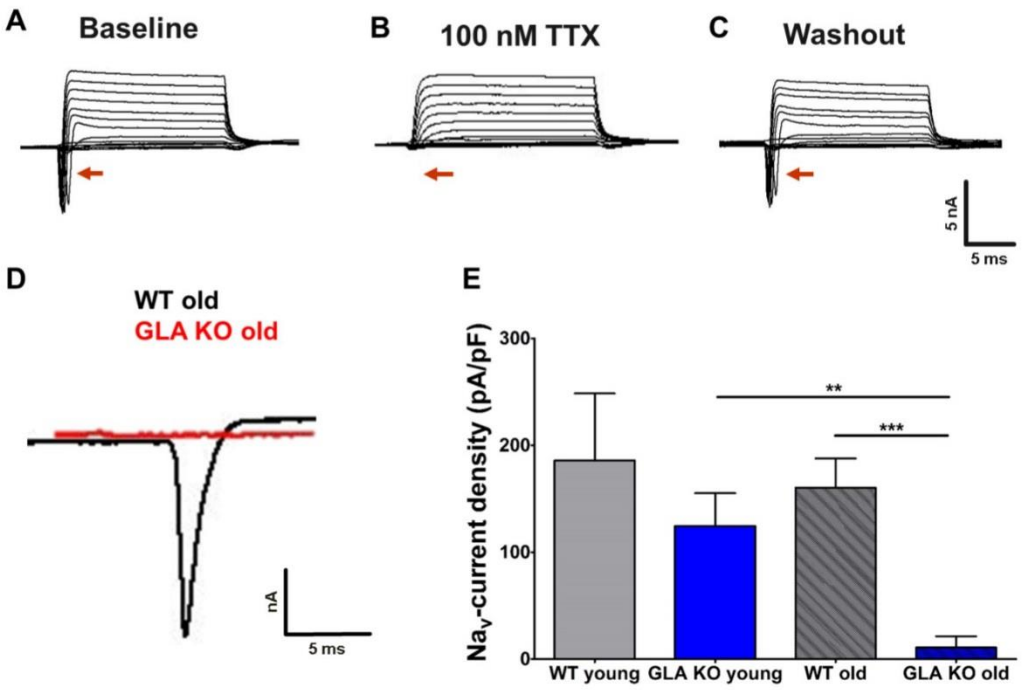

Figure 18: Quantification of current density of sodium currents and tetrodotoxin sensitivity
Graphs show sodium currents from dorsal root ganglion (DRG) neurons of a young α-GAL deficient (GLA KO) mouse in the tetrodotoxin (TTX) sensitivity test. Graphs display exemplified sodium currents of old wildtype littermate (WT) and old GLA KO mice at -30 mV. Bar graphs show the results of the quantification of sodium currents in young (3 months) and old (12-24 months) GLA KO and WT mice. Sodium currents showed fast inactivation kinetics at baseline (A, red arrow). After adding 100 nM TTX to the bath solution, sodium currents were completely blocked (B, red arrow). Washout of TTX resulted in total recover of sodium currents (C, red arrow). Currents of DRG neurons were assessed using whole-cell patch clamp analysis after three to eight days cultivation of neurons, depending on axonal growth. D) Exemplified sodium currents of old WT and old GLA KO mice. There was no difference in current densities of sodium currents (E) comparing young GLA KO mice with young and old WT mice, while sodium currents of old GLA KO mice were reduced compared to young GLA KO ($p<0.01$) and old WT mice ($p<0.001$). GLA KO: young (3 months), old (12-24 months). WT: young (3 months), old (12-24 months). At least nine cells per genotype and age-group from at least three different mice each were analyzed. **$p<0.01$; ***$p<0.001$. Arrows point to sodium currents.

There was no difference in I_h current density between young GLA KO (exemplified current Fig. 19A, B) and young and old WT mice, similar to sodium currents. DRG neurons of old GLA KO mice, however, displayed lower I_h current amplitudes compared to young GLA KO and old WT mice ($p<0.001$ each; Fig. 19C).

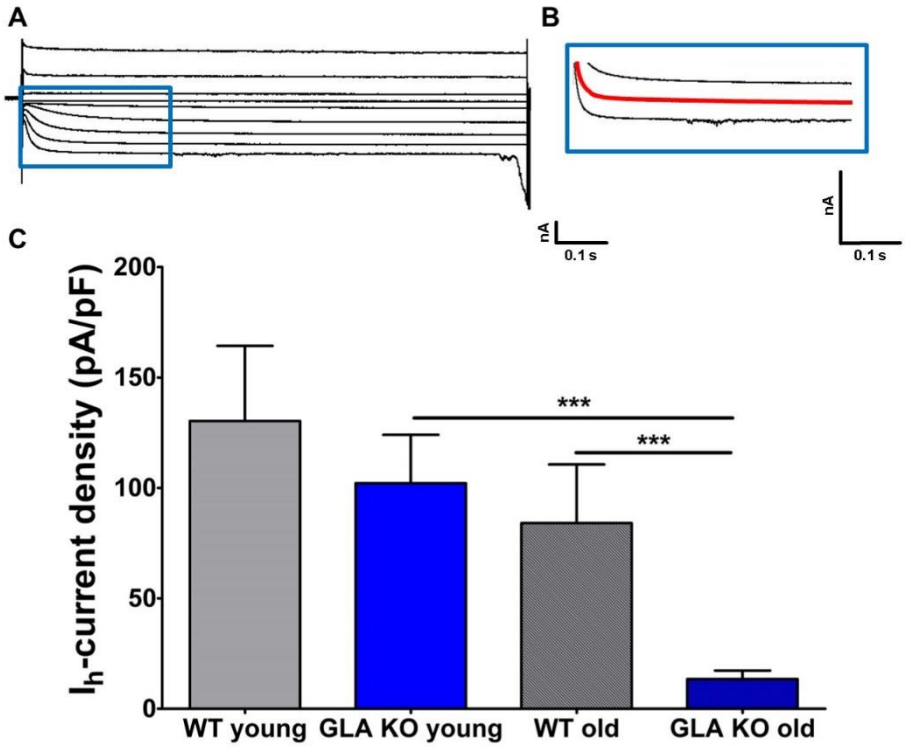

Figure 19: Quantification of I_h current density in mouse dorsal root ganglion neurons
Graphs display exemplified I_h currents of a young α-GAL deficient (GLA KO) mouse. Bar graphs show the results of the quantification of I_h currents in young (3 months) and old (12-24 months) GLA KO and wildtype littermate (WT) mice. Exemplified family of I_h currents of a young GLA KO mouse (A) and at -120 mV (B, blue box, red current). C) I_h current density did not differ between young GLA KO mice, WT littermates, and old WT mice. Old GLA KO mice displayed reduced I_h current densities compared to young GLA KO and old WT mice ($p<0.001$). GLA KO: young (3 months), old (12-24 months). WT: young (3 months), old (12-24 months). At least nine cells per genotype and age-group from at least three different mice each were analyzed. ***$p<0.001$.

5.11 No difference in TRPV1 currents in the young age-group

For characterization of capsaicin sensitive TRPV1 currents in cultured DRG neurons (exemplified current Fig. 20A), current densities were calculated as described above. We found no difference in TRPV1 current densities between young WT and young GLA KO mice (Fig. 20B), while DRG neurons of old mice did not respond to capsaicin stimulation at all (data not shown).

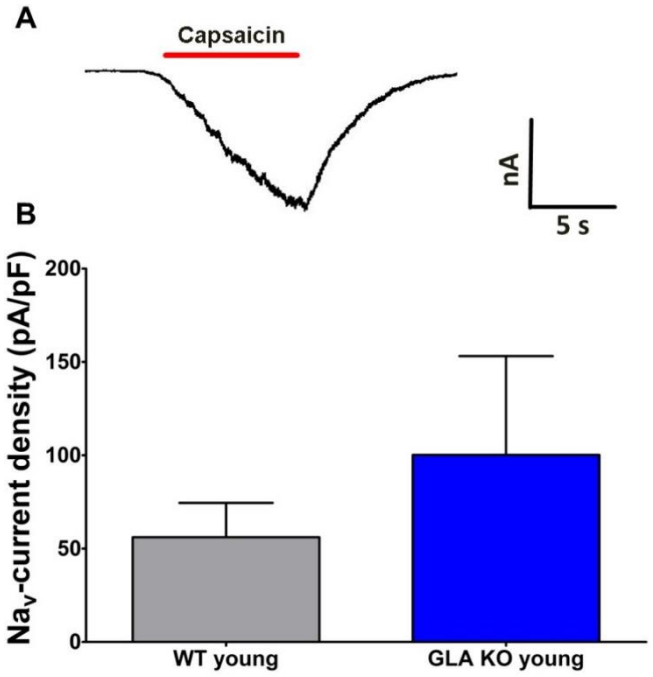

Figure 20: Quantification of TRPV1 current density in mouse dorsal root ganglion neurons
Graph displays exemplified TRPV1 current of a young α-GAL deficient (GLA KO) mouse after application of bath solution and 500 nM capsaicin. Bar graphs show the results of the quantification of TRPV1 currents in young (3 months) GLA KO and wildtype littermate (WT) mice. A) Exemplified TRPV1 current of a young GLA KO mouse after application of 500 nM capsaicin (red bar) and washout with bath solution. B) TRPV1 current density did not differ between young GLA KO mice and WT littermates. Neurons of the old age-group did not respond to applied capsaicin. GLA KO: young (3 months, n=4), WT: young (3 months, n=3).

5.12 Gb3 accumulation and Na$_v$1.7 current dysregulation in HEK cells after shRNA treatment

HEK cells transfected with control shRNA (control HEK cells; Fig. 21A-C) showed no Gb3 deposition, while HEK cells transfected with shRNA against α-Gal A (shRNA HEK cells; Fig. 21D-F) as an in vitro model for FD, displayed increased Gb3 accumulation within one week after transfection. Deposition of Gb3 was markedly decreased after HEK cell incubation with agalsidase-alpha for 24 hours (Fig. 21G-I). Quantification of Na$_v$1.7 currents revealed lower sodium current densities in shRNA HEK cells compared to control HEK cells ($p<0.01$) and control HEK cells treated with agalsidase-alpha ($p<0.05$; Fig. 21C). ShRNA HEK cells treated with agalsidase-alpha 24 hours prior to patch clamp analysis displayed no difference in sodium current densities compared to both control HEK cell groups (Fig. 21J).

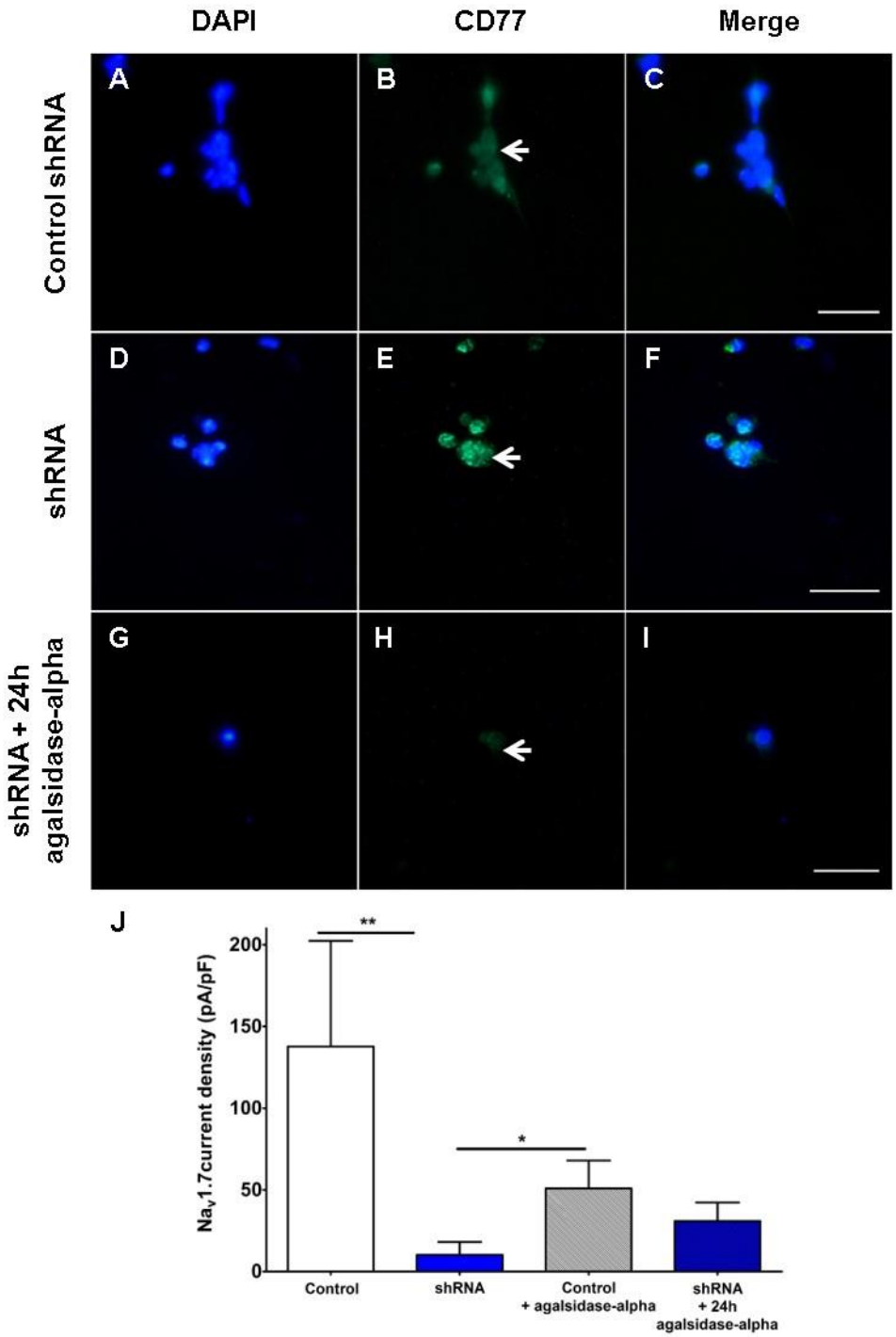

Figure 21: Knock-down of alpha galactosidase A in Na$_v$1.7 expressing HEK cells

Photomicrographs show immunoreactivity of antibodies against CD77 as a marker for Gb3 in human embryonic kidney 293 (HEK) cells expression voltage-gated sodium channel 1.7 (Na$_v$1.7) after one week of transfection with control shRNA (control HEK cells) (B, arrows), shRNA against α-galactosidase A (shRNA HEK cells) (E, arrows) and shRNA transfected HEK cells incubated with agalsidase-alpha for 24 hours (H, arrows). J) ShRNA HEK cells displayed a loss of Na$_v$1.7 sodium currents compared to control HEK cells ($p<0.01$), while shRNA HEK cells treated with agalsidase-alpha for 24 hours showed no difference compared to control cells. Arrows point to immune-positive cells. Scale bar 50 µm. *$p<0.05$, **$p<0.01$.

6. Discussion

6.1 Summary of main results

We investigated the mechanisms underlying sensory disturbance and pain in FD and characterized affective and cognitive behavior using the α-GAL deficient mouse as a model (Ohshima et al., 1995). We report on a reduction of $Na_v1.7$ currents following Gb3 accumulation in sensory DRG neurons providing a potential pathomechanism for FD-associated sensory impairment and pain.

6.2 Behavioral characterization of the GLA KO mouse under potential Fabry-associated pain conditions

6.2.1 Characterization of pain associated behavior in the GLA KO mouse

As described earlier (Lakoma et al., 2014; Rodrigues et al., 2008; Üçeyler et al., 2016), the GLA KO mouse age-dependently develops thermal hyposensitivity, while remaining hypersensitive for mechanical stimuli without sex differences and motor dysfunction in the naïve state. Since Fabry-associated pain is typically triggerable (Burlina et al., 2011; Germain, 2010), we investigated pain behavior of the GLA KO mouse after i.pl. CFA injection and CCI surgery as models of inflammatory and neuropathic pain. We demonstrate that in contrast to young GLA KO and old WT mice, old GLA KO mice, do not develop thermal and mechanical sensitivity after experimental inflammation. Additionally, there was also no increase of thermal and mechanical sensitivity in old GLA KO mice after CCI surgery compared to old WT mice. Thus, old GLA KO mice not only display thermal hyposensitivity in the naïve state (Üçeyler et al., 2016) mirroring the elevated thermal thresholds in FD patients as assessed with QST (Üçeyler et al., 2011), but are also protected from pain after inflammation and nerve lesion.

6.2.2 Characterization of affective and cognitive behavior of the GLA KO mouse.

Anxiety, depression, and cognitive impairment are symptoms frequently reported by FD patients (Bolsover et al., 2014; Laney et al., 2010; MacDermot et al., 2001b; Miners et al., 2002; Sigmundsdottir et al., 2014). We assessed anxiety-like behavior in three different tests (EPM, LDB, OF) before and after CFA treatment (Chen et al.,

2010; Stein et al., 1988) to investigate if GLA KO mice show signs of affective disturbance. Depression-like and learning behavior was examined only in the naïve state. Because the intra-individual outcome variation is particularly high in anxiety tests for animals (Ramos, 2008), we applied three different assays. The comparison of anxiety-like behavior between genotype- and age-groups in the naïve state did not reveal any relevant differences. Particularly in GLA KO mice, CFA injection resulted in an increase in anxiety-like behavior, however, only in the EPM test, while GLA KO and WT mice displayed no differences in anxiety-like behavior in the LDB and the OF. One reason might be that all three settings are exploration-based tests for anxiety-like behavior. Thus, diverse results in EPM, LDB, and OF for anxiety-like behavior are plausible due to the differences in environmental settings of the assays used (e.g. illuminated box in the LDB versus no light stimulus in the EPM test) (Hofmann et al., 2017). This diversity rather underlines that multiple tests performed at different time points are essential, because each mouse can show differences in affective behavior during the test phase and therefore it is necessary to interpret results after summary of the obtained data (Cryan and Holmes, 2005; Finn et al., 2003; Ramos, 2008). It is of note that we injected a rather low CFA concentration (20 ng/ml/injection). Using a higher CFA concentration (e.g. 1 mg/ml/injection) as reported in previous studies (Refsgaard et al., 2016) may have had resulted in consistent anxiety-like behavior in more than one test paradigm, but we used the same CFA concentration as in the pain associated behavior to test the mice in comparable conditions. Additionally, we found no genotype differences in depression-like and learning behavior. Therefore, we conclude that affective and cognitive symptoms in FD patients may not be the result of genetic influence, but rather of other environmental and epigenetic reasons (Hofmann et al., 2017).

6.3 Neuronal gene and protein expression of pain related ion channels and Gb3 accumulation in DRG neurons

To investigate if potential ion channel expression patterns underlie the FD sensory phenotype we assessed neuronal gene and protein expression of pain related ion channels in the naïve state and in the mouse model of inflammatory pain. We found no differences in gene expression of TRPV1, HCN2, $Na_v1.7$, and $Na_v1.8$ between genotypes, age- and treatment groups, indicating that ion channel gene expression might not contribute to the observed age-dependent differences of pain behavior in

the GLA KO mouse. Another explanation might be that we investigated gene expression seven days after CFA injection and changes in gene expression might have been more prominent at earlier time points (Waxman and Zamponi, 2014).

On the other hand, altered protein expression and/or functional changes of the respective ion channels in old GLA KO mice might lead to alterations in nociceptive perception. It was reported, that protein expression of TRPV1 in nociceptors (Lakoma et al., 2016b) and cutaneous TRPV1 and Nav1.8 (Lakoma et al., 2014) is increased in young α-GAL A deficient mice. In contrast to this, we found higher protein expression of TRPV1 in DRG neurons only in old GLA KO mice compared to WT littermates, but no other investigated ion channel protein expression seemed to be dysregulated in the GLA KO mice. These results lead to the conclusion that functional ion channel impairment might underlie the observed heat and mechanical insensitivity of old GLA KO mice at baseline, after i.pl. CFA injection, and after CCI. Further, we demonstrated that Gb3 age-dependently accumulates in the cytoplasm of DRG neurons of GLA KO mice. Previously it was shown in vitro that Gb3 and lyso-Gb3 enhanced voltage-gated calcium currents of sensory DRG neurons and led to mechanical allodynia when injected i.pl. in WT mice (Choi et al., 2015) supporting the hypothesis that Gb3 accumulation may influence the regulation of neuronal ion channel function.

6.4 Altered ion channel function in cultured DRG neurons

We analyzed the electrophysiological properties of DRG neurons and found a decrease of sodium currents and I_h currents in old GLA KO mice compared to young GLA KO mice and WT littermates. Voltage-gated sodium channels are associated with several pain syndromes and congenital insensitivity to pain (Cox et al., 2006; Dib-Hajj et al., 2013; Dib-Hajj and Waxman, 2014; Hoeijmakersa et al., 2015; Waxman et al., 2014), and HCN channels are pivotal contributors to neuronal excitability and rhythmicity (Benarroch, 2013). Especially, HCN2 plays a central role in small nociceptors as an action potential pacemaker in neuropathic and inflammatory pain conditions (Acosta et al., 2012; Emery et al., 2011; Papp et al., 2010; Richards and Dilley, 2015; Smith et al., 2015; Weng et al., 2012). Decrease of sodium and I_h currents seem to underlie thermal and mechanical hyposensitivity of old GLA KO mice in the naïve state and in the inflammatory and neuropathic pain models, since we did not find alterations in ion channel gene or protein expression

suitable for the behavioral phenotype. Our results indicate a potential mechanism leading to functional impairment in FD patients (Maag et al., 2008; Tavakoli et al., 2009; Üçeyler et al., 2011; Üçeyler et al., 2013). Although a previous study reported on increased TRPV1 currents in cultured DRG neurons of young GLA KO compared to WT littermates (Lakoma et al., 2016b), we could not detect any differences between genotypes in this age-group. In this study we stimulated cultivated neurons with a rather low capsaicin concentration of 500 nM and calculated current density related to the size of each cell. In contrast to this Lakoma et. al stimulated their neurons with 1 µM capsaicin and used WT mice of unknown background, which might explain these contrary results.

6.5 Influence of Gb3 accumulation on $Na_v1.7$ channel function

We analyzed electrophysiological properties of the $Na_v1.7$ channel in an in vitro model for FD, as a potential proof of principle that Gb3 deposition directly influences ion channel function. Choi et al. showed that, besides the potential amplification of voltage-gated calcium currents (Choi et al., 2015), lyso-Gb3 also inhibits synthesis and surface expression of the calcium-activated potassium channel KCa3.1 in fibroblasts (Choi and Park, 2016). This provides evidence for the influence of Gb3 on ion channel expression and function. We now show functional alterations in Nav1.7 channels that are strongly associated with nociception and pain. Our results provide first evidence for a potential direct dysregulation of neuronal ion channels as demonstrated for $Na_v1.7$ by intracellular Gb3, as a concept for functional neuronal impairment in FD.

6.6 Potential mechanism underlying sensory impairment, pain, and small fiber neuropathy in FD

Based on our results we propose a potential mechanism of sensory impairment, pain, and small fiber degeneration in FD (Fig. 22).We demonstrated that old GLA KO display reduced thermal and mechanical sensitivity not only in the naïve state (Üçeyler et al., 2016), but also after inflammation and nerve lesion. Gb3 accumulation in DRG neurons may directly dysregulate pain related ion channel function, as exemplified for $Na_v1.7$.

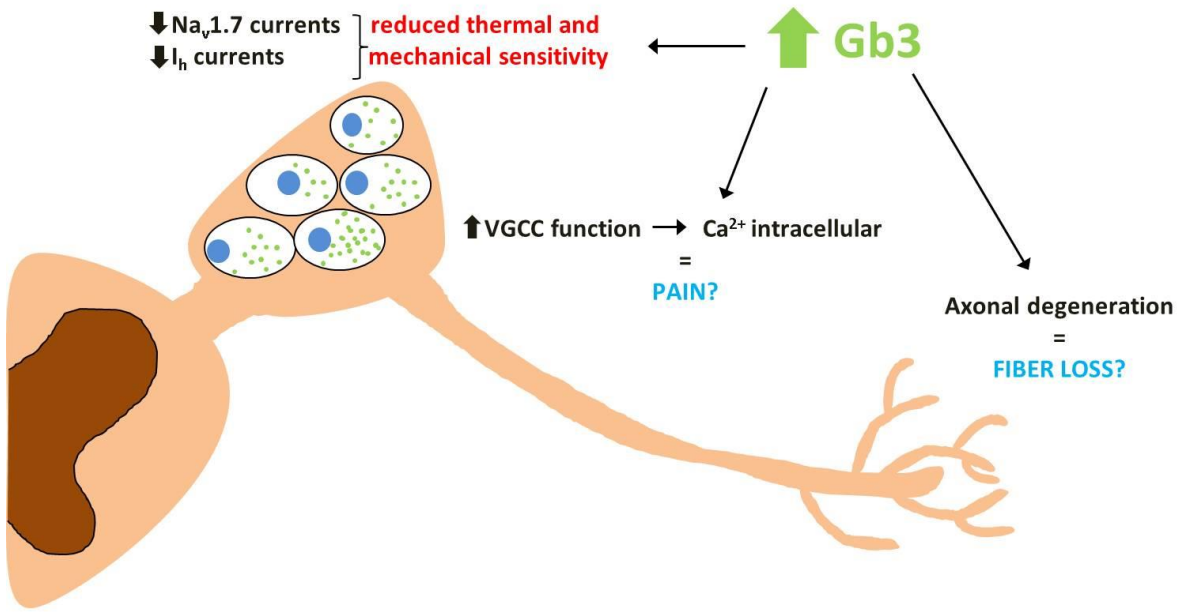

Figure 22: Potential mechanism underlying sensory disturbance and nerve fiber degeneration in FD

Graph displays potential mechanism for pain and small fiber degeneration in Fabry disease (FD). Globotriaosylceramide (Gb3, green) accumulates in dorsal root ganglion (DRG) neurons due to deficiency of the enzyme α-galactosidase A. This deposition leads to a reduction of sodium and decrease of I_h currents, resulting in reduced thermal and mechanical sensitivity. Gb3 accumulation in DRG neurons may also lead to an increase of voltage-gated calcium channel function, which might contribute to Fabry-associated pain. Additionally, Gb3 deposition may also lead to increased cellular stress reaction, resulting in axonal degeneration, which starts in small diameter intra epidermal nerve fibers (IENF).

Reduction of sodium and I_h currents might contribute to the observed age-dependent differences of pain behavior in the GLA KO mouse and to elevated thermal thresholds in FD patients (Üçeyler et al., 2011). On the other hand, we found no hints for spontaneous or induced hyperactivity or hyperexcitability of the examined ion channels and the mechanism leading to FD pain remains elusive. One potential contributor may be the voltage-gated calcium channels. The increase of intracellular calcium and sensitization of these channels through neuronal Gb3 accumulation (Choi et al., 2015) might be a relevant trigger. Altered ion channel function may be due to Gb3 dependent dysregulation of neuronal ion channel synthesis, membrane expression, and anchoring (Maalouf et al., 2010). In human fibroblasts, cyclic adenosine monophosphate (cAMP) was increased via lyso-Gb3 by upregulation of adenylyl-cyclase-6. Lyso-Gb3 also inhibited ERK 1/2 phosphorylation by the protein

kinase A (PKA) pathway, resulting in inhibited KCa3.1 channel synthesis. Additionally, the expression of class II phosphatidylinositol 3-kinase C2β by PKA activation is also suppressed by lyso-Gb3, which reduces the production of phosphatidylinositol 3-phosphate (PI(3)P). This reduction led to reduced membrane surface expression of KCa3.1 channels, which was recovered by increasing the intracellular levels of PI(3)P (Choi and Park, 2016). Another potential pathway leading to altered ion channel function may be the inhibition of PKA. Herrmann et al. reported that inhibition of PKA function via mutation suppressed cAMP mediated HCN2 sensitization in nociceptive sensory neurons under inflammatory pain conditions (Herrmann et al., 2017). Gb3 deposition might lead to PKA activation as described earlier (Choi and Park, 2016), inhibiting HCN2 regulatory function. Additionally, it was shown that increased cAMP levels facilitate HCN2 activation and repetitive firing in primary nociceptive nerve fibers in diabetes-associated pain (Tsantoulas and Lainez, 2017). These findings determine HCN2 as an additional key player in FD sensory impairment. As exemplified for $Na_v1.7$ currents in our in vitro model, ERT with agalsidase-alpha reversed reduction of sodium currents, caused by Gb3 accumulation. FD patients, in contrast, display diverse response of to ERT (Schiffmann, 2010; Üçeyler et al., 2011) which might be due to disease persistence for many years until diagnosis and start of ERT (Mehta et al., 2010). Ion channel impairment might be therefore permanent. Additionally, similar to FD patients (Burlina et al., 2011; Üçeyler et al., 2011), young GLA KO mice revealed a reduction of intraepidermal nerve fiber density (Lakoma et al., 2014). The reduction of the peripheral nerve endings of dorsal root ganglion neurons might be due to the potential neurotoxic effects of Gb3 accumulations and its metabolites (Jeyakumar et al., 2002; Shen et al., 2008), which might lead to apoptosis starting in small diameter neurons.

6.7 Outlook

Our results provide evidence for Gb3-dependent Nav1.7 impairment in sensory DRG neurons as a potential contributor to sensory dysfunction and pain in FD. Further studies are needed to clarify the potential relevance of these findings in human patients, to identify distinct ion channels involved in Fabry-associated pain and to elucidate the role of Gb3 accumulations contributing in neuronal cell death. Deciphering the underlying pathomechanism will provide the basis for the development of more targeted treatment approaches in FD patients.

7. References

Acosta, C., et al., 2012. HCN1 and HCN2 in Rat DRG neurons: levels in nociceptors and non-nociceptors, NT3-dependence and influence of CFA-induced skin inflammation on HCN2 and NT3 expression. PLoS One. 7**,** e50442.

Allen, A.L., Cortright, D.N., McCarson, K.E., 2003. Formalin- or adjuvant-induced peripheral inflammation increases neurokinin-1 receptor gene expression in the mouse. Brain Res. 961**,** 147-52.

Anderson, W., 1898. A case of "Angeio-Keratoma". British Journal of Dermatology. Volume 10**,** 113-117.

Askari, H., et al., 2007. Cellular and tissue localization of globotriaosylceramide in Fabry disease. Virchows Arch. 451**,** 823-34.

Balwani, M., et al., 2009. Use of complementary and alternative medicine by patients with lysosomal storage diseases. Genet Med. 11**,** 722-7.

Bangari, D.S., et al., 2015. alpha-Galactosidase A knockout mice: progressive organ pathology resembles the type 2 later-onset phenotype of Fabry disease. Am J Pathol. 185**,** 651-65.

Benarroch, E.E., 2013. HCN channels: function and clinical implications. Neurology. 80**,** 304-10.

Bennett, G.J., Xie, Y.K., 1988. A peripheral mononeuropathy in rat that produces disorders of pain sensation like those seen in man. Pain. 33**,** 87-107.

Biancini, G.B., et al., 2017. Globotriaosylsphingosine induces oxidative DNA damage in cultured kidney cells. Nephrology (Carlton). 22**,** 490-493.

Biegstraaten, M., et al., 2015. Recommendations for initiation and cessation of enzyme replacement therapy in patients with Fabry disease: the European Fabry Working Group consensus document. Orphanet J Rare Dis. 10**,** 36.

Bishop, D.F., Kornreich, R., Desnick, R.J., 1988. Structural organization of the human alpha-galactosidase A gene: further evidence for the absence of a 3' untranslated region. Proc Natl Acad Sci U S A. 85**,** 3903-7.

Bolsover, F.E., et al., 2014. Cognitive dysfunction and depression in Fabry disease: a systematic review. J Inherit Metab Dis. 37**,** 177-87.

Bourinet, E., et al., 2014. Calcium-permeable ion channels in pain signaling. Physiol Rev. 94**,** 81-140.

Brady, R.O., et al., 1967. Enzymatic defect in Fabry's disease. Ceramidetrihexosidase deficiency. N Engl J Med. 276**,** 1163-7.

Breese, N.M., et al., 2005. Peripheral inflammation selectively increases TRPV1 function in IB4-positive sensory neurons from adult mouse. Pain. 115**,** 37-49.

Brenner, D.S., Golden, J.P., Gereau, R.W.t., 2012. A novel behavioral assay for measuring cold sensation in mice. PLoS One. 7**,** e39765.

Brouwer, B.A., et al., 2014. Painful neuropathies: the emerging role of sodium channelopathies. J Peripher Nerv Syst. 19**,** 53-65.

Burlina, A.P., et al., 2011. Early diagnosis of peripheral nervous system involvement in Fabry disease and treatment of neuropathic pain: the report of an expert panel. BMC Neurol. 11**,** 61.

Carandang, R., et al., 2006. Trends in incidence, lifetime risk, severity, and 30-day mortality of stroke over the past 50 years. Jama. 296**,** 2939-46.

Caterina, M.J., et al., 1997. The capsaicin receptor: a heat-activated ion channel in the pain pathway. Nature. 389**,** 816-24.

Caterina, M.J., et al., 2000. Impaired Nociception and Pain Sensation in Mice Lacking the Capsaicin Receptor. Science. 288**,** 306-313.

Chaplan, S.R., et al., 1994. Quantitative assessment of tactile allodynia in the rat paw. J Neurosci Methods. 53**,** 55-63.

Chen, Y., et al., 2010. Nitric oxide synthase modulates CFA-induced thermal hyperalgesia through cytokine regulation in mice. Mol Pain. 6**,** 13.

Choi, J.Y., Park, S., 2016. Role of protein kinase A and class II phosphatidylinositol 3-kinase C2beta in the downregulation of KCa3.1 channel synthesis and membrane surface expression by lyso-globotriaosylceramide. Biochem Biophys Res Commun. 470**,** 907-12.

Choi, L., et al., 2015. The Fabry disease-associated lipid Lyso-Gb3 enhances voltage-gated calcium currents in sensory neurons and causes pain. Neurosci Lett. 594**,** 163-8.

Cox, J., et al., 2006. An SCN9A channelopathy causes congenital inability to experience pain. Nature. 444(7121)**,** 894-8.

Crawley, J., Goodwin, F.K., 1980. Preliminary report of a simple animal behavior model for the anxiolytic effects of benzodiazepines. Pharmacol Biochem Behav. 13**,** 167-70.

Cryan, J.F., Holmes, A., 2005. The ascent of mouse: advances in modelling human depression and anxiety. Nat Rev Drug Discov. 4**,** 775-90.

De Francesco, P.N., et al., 2013. Fabry disease peripheral blood immune cells release inflammatory cytokines: Role of globotriaosylceramide. Mol Genet Metab.

Dib-Hajj, S.D., et al., 2005. Gain-of-function mutation in Nav1.7 in familial erythromelalgia induces bursting of sensory neurons. Brain. 128**,** 1847-54.

Dib-Hajj, S.D., et al., 2009. Voltage-gated sodium channels in pain states: role in pathophysiology and targets for treatment. Brain Res. Rev. 60**,** 65–83.

Dib-Hajj, S.D., et al., 2013. The NaV1.7 sodium channel: from molecule to man. Nature Reviews Neuroscience. 14**,** pp. 49–62.

Dib-Hajj, S.D., Waxman, S.G., 2014. Translational pain research: Lessons from genetics and genomics. Sci Transl Med. 6**,** 249sr4.

Echevarria, L., et al., 2015. X-chromosome inactivation in female patients with Fabry disease. Clin Genet.

Emery, E.C., et al., 2011. HCN2 ion channels play a central role in inflammatory and neuropathic pain. Science. 333**,** 1462-6.

Faber, C.G., et al., 2012. Gain-of-function Nav1.8 mutations in painful neuropathy. Proc Natl Acad Sci U S A. 109**,** 19444-9.

Fabry, J., 1898. Ein Beitrag zur Kenntniss der Purpura haemorrhagica nodularis (Purpura papulosa haemorrhagica Hebrae). Dermatol. Wochenschr. 43**,** 187-300.

Fellgiebel, A., et al., 2014. Enzyme replacement therapy stabilized white matter lesion progression in Fabry disease. Cerebrovasc Dis. 38**,** 448-56.

Fertleman, C., et al., 2006. SCN9A mutations in paroxysmal extreme pain disorder: allelic variants underlie distinct channel defects and phenotypes. Neuron. 52(5)**,** 767-74.

Finn, D.A., Rutledge-Gorman, M.T., Crabbe, J.C., 2003. Genetic animal models of anxiety. Neurogenetics. 4**,** 109-35.

Gadoth, N., Sandbank, U., 1983. Involvement of dorsal root ganglia in Fabry's disease. J Med Genet. 20**,** 309-12.

Germain, D.P., 2010. Fabry disease. Orphanet J Rare Dis. 5**,** 30.

Germain, D.P., et al., 2016. Treatment of Fabry's Disease with the Pharmacologic Chaperone Migalastat. N Engl J Med. 375**,** 545-55.

Hamill, O.P., et al., 1981. Improved patch-clamp techniques for high-resolution current recording from cells and cell-free membrane patches. Pflugers Arch. 391**,** 85-100.

Hargreaves, K., et al., 1988. A new and sensitive method for measuring thermal nociception in cutaneous hyperalgesia. Pain. 32**,** 77-88.

Herrmann, S., et al., 2017. Protein kinase A regulates inflammatory pain sensitization by modulating HCN2 channel activity in nociceptive sensory neurons. Pain. 158**,** 2012-2024.

Hoeijmakersa, J.G.J., et al., 2015. Painful peripheral neuropathy and sodium channel mutations. Neuroscience Letters. 596**,** 51-59.

Hofmann, L., et al., 2017. Affective and cognitive behavior in the alpha-galactosidase A deficient mouse model of Fabry disease. PLoS One. 12**,** e0180601.

Hughes, D.A., et al., 2017. Oral pharmacological chaperone migalastat compared with enzyme replacement therapy in Fabry disease: 18-month results from the randomised phase III ATTRACT study. J Med Genet. 54**,** 288-296.

Hwu, W.L., et al., 2009. Newborn screening for Fabry disease in Taiwan reveals a high incidence of the later-onset GLA mutation c.936+919G>A (IVS4+919G>A). Hum Mutat. 30**,** 1397-405.

Inoue, T., et al., 2013. Newborn screening for Fabry disease in Japan: prevalence and genotypes of Fabry disease in a pilot study. J Hum Genet. 58**,** 548-52.

Jeyakumar, M., et al., 2002. Glycosphingolipid lysosomal storage diseases: therapy and pathogenesis. Neuropathol Appl Neurobiol. 28**,** 343-57.

Kawagoe, S., et al., 2013. Morphological features of iPS cells generated from Fabry disease skin fibroblasts using Sendai virus vector (SeVdp). Mol Genet Metab. 109**,** 386-9.

Kaye, E.M., et al., 1988. Nervous system involvement in Fabry's disease: clinicopathological and biochemical correlation. Ann Neurol. 23**,** 505-9.

Keslova-Veselikova, J., et al., 2008. Replacement of alpha-galactosidase A in Fabry disease: effect on fibroblast cultures compared with biopsied tissues of treated patients. Virchows Arch. 452**,** 651-65.

Kolodny, E., et al., 2015. Cerebrovascular involvement in Fabry disease: current status of knowledge. Stroke. 46**,** 302-13.

Lai, J., Hunter, J.C., Porreca, F., 2003. The role of voltage-gated sodium channels in neuropathic pain. Curr Opin Neurobiol. 13**,** 291-7.

Lakoma, J., et al., 2014. Pain related channels are differentially expressed in neuronal and non-neuronal cells of glabrous skin of fabry knockout male mice. PLoS One. 9**,** e108641.

Lakoma, J., et al., 2016a. Characterization of Human Dermal Fibroblasts in Fabry Disease. J Cell Physiol. 231**,** 192-203.

Lakoma, J., et al., 2016b. Increased expression of Trpv1 in peripheral terminals mediates thermal nociception in Fabry disease mouse model. Mol Pain. 12.

Laney, D.A., et al., 2010. Social-adaptive and psychological functioning of patients affected by Fabry disease. J Inherit Metab Dis. 33 Suppl 3**,** S73-81.

Lelieveld, I.M., et al., 2015. Eight-Year Follow-Up of Neuropsychiatric Symptoms and Brain Structural Changes in Fabry Disease. PLoS One. 10**,** e0137603.

Lidove, O., et al., 2007. Clinical results of enzyme replacement therapy in Fabry disease: a comprehensive review of literature. Int J Clin Pract. 61**,** 293-302.

Löhle, M., et al., 2015. Clinical prodromes of neurodegeneration in Anderson-Fabry disease. Neurology. 84**,** 1454-64.

Maag, R., Binder, A., Baron, R., 2008. Assessment of pain and somatosensory function in Fabry disease: early diagnosis. Clin Ther. 30 Suppl B**,** S52-3.

Maalouf, K., et al., 2010. A modified lipid composition in Fabry disease leads to an intracellular block of the detergent-resistant membrane-associated dipeptidyl peptidase IV. Journal of Inherited Metabolic Disease. 33**,** 445-449.

MacDermot, K.D., Holmes, A., Miners, A.H., 2001a. Natural history of Fabry disease in affected males and obligate carrier females. J Inherit Metab Dis. 24 Suppl 2**,** 13-4; discussion 11-2.

MacDermot, K.D., Holmes, A., Miners, A.H., 2001b. Anderson-Fabry disease: clinical manifestations and impact of disease in a cohort of 98 hemizygous males. J Med Genet. 38**,** 750-60.

Marshall, J., et al., 2010. Substrate reduction augments the efficacy of enzyme therapy in a mouse model of Fabry disease. PLoS One. 5**,** e15033.

Matsuyoshi, H., et al., 2006. Expression of hyperpolarization-activated cyclic nucleotide-gated cation channels in rat dorsal root ganglion neurons innervating urinary bladder. Brain Res. 1119**,** 115-23.

Mehta, A., et al., 2010. Fabry disease: a review of current management strategies. QJM. 103**,** 641-59.

Meikle, P.J., et al., 1999. Prevalence of lysosomal storage disorders. Jama. 281**,** 249-54.

Miners, A.H., et al., 2002. Assessment of health-related quality-of-life in males with Anderson Fabry Disease before therapeutic intervention. Qual Life Res. 11**,** 127-33.

Morris, R., 1984. Developments of a water-maze procedure for studying spatial learning in the rat. J Neurosci Methods. 11**,** 47-60.

Motabar, O., et al., 2010. Fabry disease - current treatment and new drug development. Curr Chem Genomics. 4**,** 50-6.

Nakagawa, M., et al., 2008. Generation of induced pluripotent stem cells without Myc from mouse and human fibroblasts. Nat Biotechnol. 26**,** 101-6.

Namer, B., et al., 2017. Changes in Ionic Conductance Signature of Nociceptive Neurons Underlying Fabry Disease Phenotype. Front Neurol. 8**,** 335.

Nassar, M.A., et al., 2005. Neuropathic pain develops normally in mice lacking both Na(v)1.7 and Na(v)1.8. Mol Pain. 1**,** 24.

Ohshima, T., et al., 1995. Structural organization and expression of the mouse gene encoding alpha-galactosidase A. Gene. 166**,** 277-80.

Ohshima, T., et al., 1997. alpha-Galactosidase A deficient mice: a model of Fabry disease. Proc Natl Acad Sci U S A. 94**,** 2540-4.

Papp, I., Hollo, K., Antal, M., 2010. Plasticity of hyperpolarization-activated and cyclic nucleotid-gated cation channel subunit 2 expression in the spinal dorsal horn in inflammatory pain. Eur J Neurosci. 32**,** 1193-201.

Pellow, S., et al., 1985. Validation of open:closed arm entries in an elevated plus-maze as a measure of anxiety in the rat. J Neurosci Methods. 14**,** 149-67.

Persson, A.K., et al., 2013. Neuropathy-associated Nav1.7 variant I228M impairs integrity of dorsal root ganglion neuron axons. Ann Neurol. 73**,** 140-5.

Politei, J.M., et al., 2016. Pain in Fabry Disease: Practical Recommendations for Diagnosis and Treatment. CNS Neurosci Ther. 22**,** 568-76.

Porsolt, R.D., Bertin, A., Jalfre, M., 1977. Behavioral despair in mice: a primary screening test for antidepressants. Arch Int Pharmacodyn Ther. 229**,** 327-36.

Prut, L., Belzung, C., 2003. The open field as a paradigm to measure the effects of drugs on anxiety-like behaviors: a review. Eur J Pharmacol. 463**,** 3-33.

Ramos, A., 2008. Animal models of anxiety: do I need multiple tests? Trends Pharmacol Sci. 29**,** 493-8.

Refsgaard, L.K., et al., 2016. Modelling affective pain in mice: Effects of inflammatory hypersensitivity on place escape/avoidance behaviour, anxiety and hedonic state. J Neurosci Methods. 262**,** 85-92.

Richards, N., Dilley, A., 2015. Contribution of hyperpolarization-activated channels to heat hypersensitivity and ongoing activity in the neuritis model. Neuroscience. 284**,** 87-98.

Rodrigues, L.G., et al., 2008. Neurophysiological, behavioral and morphological abnormalities in the Fabry knockout mice. Neurobiol Dis. 33;48-56.

Rolfs, A., et al., 2013. Interdisciplinary guideline for the diagnosis and therapy of Fabry's disease.

Rolyan, H., et al., 2016. A painful neuropathy-associated Nav1.7 mutant leads to time-dependent degeneration of small-diameter axons associated with intracellular Ca(2+) dysregulation and decrease in ATP levels. Mol Pain. 12.

Salat, K., Moniczewski, A., Librowski, T., 2013. Transient receptor potential channels - emerging novel drug targets for the treatment of pain. Curr Med Chem. 20**,** 1409-36.

Schiffmann, R., 2009. Fabry disease. Pharmacol Ther. 122**,** 65-77.

Schiffmann, R., 2010. Agalsidase treatment for Fabry disease: uses and rivalries. Genet Med. 12**,** 684-5.

Schiffmann, R., et al., 2017. Screening, diagnosis, and management of patients with Fabry disease: conclusions from a “Kidney Disease: Improving Global Outcomes” (KDIGO) Controversies Conference. Kidney International. 91**,** 284-293.

Schindelin, J., et al., 2012. Fiji: an open-source platform for biological-image analysis. Nat Methods. 9**,** 676-82.

Shen, J.S., et al., 2008. Globotriaosylceramide induces oxidative stress and up-regulates cell adhesion molecule expression in Fabry disease endothelial cells. Mol Genet Metab.

Shiozuka, C., et al., 2011. Increased globotriaosylceramide levels in a transgenic mouse expressing human alpha1,4-galactosyltransferase and a mouse model for treating Fabry disease. J Biochem. 149**,** 161-70.

Sigmundsdottir, L., et al., 2014. Cognitive and psychological functioning in Fabry disease. Arch Clin Neuropsychol. 29**,** 642-50.

Sims, K., et al., 2009. Stroke in Fabry disease frequently occurs before diagnosis and in the absence of other clinical events: natural history data from the Fabry Registry. Stroke. 40**,** 788-94.

Sirrs, S., et al., 2016. Canadian Fabry Disease Treatment Guidelines 2016.

Smith, T., et al., 2015. Increased expression of HCN2 channel protein in L4 dorsal root ganglion neurons following axotomy of L5- and inflammation of L4-spinal nerves in rats. Neuroscience. 295**,** 90-102.

Sommer, C., Schäfers, M., 1998. Painful mononeuropathy in C57BL/Wld mice with delayed wallerian degeneration: differential effects of cytokine production and nerve regeneration on thermal and mechanical hypersensitivity. Brain Res. 784**,** 154-62.

Spada, M., et al., 2006. High incidence of later-onset fabry disease revealed by newborn screening. Am J Hum Genet. 79**,** 31-40.

Stein, C., Millan, M.J., Herz, A., 1988. Unilateral inflammation of the hindpaw in rats as a model of prolonged noxious stimulation: alterations in behavior and nociceptive thresholds. Pharmacol Biochem Behav. 31**,** 445-51.

Taguchi, A., et al., 2013. A symptomatic Fabry disease mouse model generated by inducing globotriaosylceramide synthesis. Biochem J. 456**,** 373-83.

Takenaka, T., et al., 2000. Long-term enzyme correction and lipid reduction in multiple organs of primary and secondary transplanted Fabry mice receiving transduced bone marrow cells. Proc Natl Acad Sci U S A. 97**,** 7515-20.

Tavakoli, M., et al., 2009. Corneal confocal microscopy: a novel noninvasive means to diagnose neuropathy in patients with Fabry disease. Muscle Nerve. 40**,** 976-84.

Tominaga, M., 2007. Nociception and TRP channels. Handb Exp Pharmacol. 489-505.

Toyooka, K., 2011. Fabry disease. Curr Opin Neurol. 24**,** 463-8.

Treede, R.D., et al., 2008. Neuropathic pain: redefinition and a grading system for clinical and research purposes. Neurology. 70**,** 1630-5.

Tsantoulas, C., Lainez, S., 2017. Hyperpolarization-activated cyclic nucleotide-gated 2 (HCN2) ion channels drive pain in mouse models of diabetic neuropathy. 9**,** eaam6072.

Üçeyler, N., et al., 2011. Small fibers in Fabry disease: baseline and follow-up data under enzyme replacement therapy. J Peripher Nerv Syst. 16**,** 304-14.

Üçeyler, N., Sommer, C., 2012. [Fabry disease : Diagnosis and treatment]. Schmerz. 26**,** 609-19.

Üçeyler, N., et al., 2013. Impaired small fiber conduction in patients with Fabry disease: a neurophysiological case-control study. BMC Neurol. 13**,** 47.

Üçeyler, N., et al., 2014. Characterization of pain in fabry disease. Clin J Pain. 30**,** 915-20.

Üçeyler, N., et al., 2016. Comprehensive and differential long-term characterization of the alpha-galactosidase A deficient mouse model of Fabry disease focusing on the sensory system and pain development. Mol Pain. 12.

Waxman, S.G., et al., 1999. Sodium channels, excitability of primary sensory neurons, and the molecular basis of pain. Muscle Nerve. 22**,** 1177-87.

Waxman, S.G., et al., 2014. Sodium channel genes in pain-related disorders: phenotype-genotype associations and recommendations for clinical use. Lancet Neurol. 13**,** 1152-60.

Waxman, S.G., Zamponi, G.W., 2014. Regulating excitability of peripheral afferents: emerging ion channel targets. Nat Neurosci. 17**,** 153-63.

Weng, X., et al., 2012. Chronic inflammatory pain is associated with increased excitability and hyperpolarization-activated current (Ih) in C- but not Adelta-nociceptors. Pain. 153**,** 900-14.

Yang, X., et al., 2009. Peripheral inflammation increased the synaptic expression of NMDA receptors in spinal dorsal horn. Pain. 144**,** 162-9.

Yang, Y., et al., 2004. Mutations in SCN9A encoding a sodium channel alpha subunit, in patients with primary erythermalgia. J. Med. Genet. 41**,** pp. 171–174.

Zarate, Y.A., Hopkin, R.J., 2008. Fabry's disease. Lancet. 372**,** 1427-35.

8. Appendices

8.1 Technical equipment

Analog Vortex Mixer	VWR, Radnor, USA
Biosphere Filter Tips	Sarstedt, Nuernbrecht, Germany
Balance 440-47	Kern AG, Frankfurt am Main, Germany
Borosilicate glass capillaries	Kimble Chase Life Science and Research Products, Meiningen, Germany
CCD camera	Visitron Systems, Tuchheim Germany
Centrifuges	
Centrifuge 5417R	Eppendorf, Hamburg, Germany
Rotina 420R	Hettich, Tuttlingen, Germany
Spectrafuge 3-1810	Neolab, Heidelberg, Germany
Clips	B. Braun, Melsungen, Germany
Combitips advanced 0,5 ml	Eppendorf, Hamburg, Germany
Cryostat CM 3050	Leica, Wetzlar, Germany
Incubator	
Heracell 150	Heraeus Instruments, Hanau, Germany
Falcon tubes (15 ml, 50 ml)	Greiner Bio One GmbH, Frickenhausen, Germany
Freezer comfort -20˚C	Liebherr, Biberach, Germany
Freezer TSX Series -80˚C	Thermo Scientific, Waltham, USA
Hargreaves apparatus	Ugo Basile Inc., Comerio, Italy
Heating plate	Medax, Neumünster, Germany
Homogenizer Polytron PT 1600	Kinematika AG, Luzern, Schweiz
MicroAmp® fast 96-well reaction plate	Applied Biosystems, Darmstadt, Germany
MicroAmp® adhesive film	Applied Biosystems, Darmstadt, Germany

Micropipette Puller Flaming/Brown	Sutter Instrument, Novato, USA
Microscopes	
Axiophot 2	Zeiss, Oberkochen, Germany
BH2	Olympus, Hamburg, Germany
Stemi 2000	Zeiss, Oberkochen, Germany
IX81 microscope	Olympus, Hamburg, Germany
Axiovert 35	Zeiss, Oberkochen, Germany
Multipipette stream	Eppendorf, Hamburg, Germany
NanoPhotometer Pearl®	Implen, Munich, Germany
Needle 27G	B. Braun, Melsungen, Germany
Object slides superfrost	Langenbrinck, Teningen, Germany
Optical adhesive covers	Langenbrinck, Teningen, Germany
PCR Tubes 0,2 ml, 1,5 ml	Eppendorf, Hamburg, Germany
Parafilm® M	Bemis Company Inc, Oshkosh, USA
PapPen	Sigma-Aldrich, St. Louis, USA
Pipettes	
Research plus	Eppendorf, Hamburg, Germany
Pipetman	Gilson, Bad Camberg, Germany
Software	
Anymaze version 4.99m	Stoelting, Wood Dale, USA
Fiji (Image J free software version 1.51f)	National Institute of Health, USA
Igor	WaveMetrics, Lake Oswego, USA
Office 2010	Microsoft, Redmond, USA
GraphPad Prism, version 5.03	GraphPad Software, San Diego, USA
Spot version 5.2	Spot Software BV, Amsterdam, Netherlands

SPSS IBM version 23	IBM, Ehningen, Germany
PULSE/PULSEFIT	HEKA, Ludwigsburg, Germany
Surgical Blades	B. Braun, Melsungen, Germany
Surgical cutlery	FST, Heidelberg, Germany
Suture	
7-0 Prolene	Ethicon, Somerville, USA
6/0 Silkam	B. Braun, Melsungen, Germany
5-0 Vicryl	Ethicon, Somerville, USA
Syringes 1 ml, 5 ml, 10 ml	BD, Franklin Lakes, USA
Thermocycler	
Step One Plus Real Time PCR	Applied Biosystems, Darmstadt, Germany
Peqstar	Peqlab, Erlangen, Germany
Primus 96	Peqlab, Erlangen, Germany
Tissue-Tek® Cryomold	Sakura, Staufen, Germany
Valve Commander	Scientific instruments, Gilching, Germany
Von Frey filaments	Stoelting, Wood Dale, USA

8.2 Reagents

Agalsidase-alpha	Shire, Saint Helier, UK
Agarose	Roth, Karlsruhe, Germany
Bovine serum albumine	Sigma-Aldrich, Taufkirchen, Germany
Capsaicin	Merck Millipore, Darmstadt, Germany
Diethylpyrocarbonate (DEPC)	Sigma-Aldrich, Taufkirchen, Germany
Ethanol	Sigma-Aldrich, Taufkirchen, Germany
Geneticin (G418)	Life Technologies, Carlsbad, USA
Gentamicin	Sigma-Aldrich, Taufkirchen, Germany

Isoflurane CP®	CP Pharma, Burgdorf, Germany
Kapa2G fast PCR Kit	Kapa Biosystems, Wilmington, USA
Liberase DL	Roche, Rotkreuz, Switzerland
Lipofectamine 3000 Transfection Kit	Invitrogen, Carlsbad, USA
2-Methylbutane	Carl Roth, Karlsruhe, Germany
$Na_v1.7$ ELISA kit	BlueGene, Shanghai, China
Nuclease free water	Applied Biosystems, Darmstadt, Germany
ROX Reference Dye	Invitrogen, Carlsbad, USA
ShRNA Bacterial TRC2 library	Sigma-Aldrich, Taufkirchen, Germany
Sodium chloride solution 0,9%	Merck Millipore, Darmstadt, Germany
TagMan Universal PCR master Mix	Applied Biosystems, Darmstadt, Germany
Tetrodotoxin (TTX)	Alomone Labs, Jerusalem, Israel
TRIzol reagent	Life Technologies, Carlsbad, USA
Trypsin-EDTA 0.05%	Life Technologies, Carlsbad, USA

8.3 Buffers and solutions

DEPC-H_2O	0.01% DEPC Dissolve in distilled water, autoclave
PBS (1x)	137 mM NaCl 2.7 mM KCL 1.5 mM KH_2PO_4 8.1 mM Na_2PO_4 pH 7.4

Bath solution (DRG)	135 mM NaCl
	5.4 mM KCl
	1.8 mM CaCl2
	1 mM MgCl2
	10 mM glucose
	5 mM HEPES
Bath solution (HEK)	140 mM NaCl
	3mM KCl
	1mM CaCl2
	1 mM MgCL2
	10 mM HEPES
Pipette recording solution (DRG)	140 mM KCl
	2 mM $MgCl_2$
	1 mM EGTA
	1 mM ATP
	5 mM HEPES
Pipette recording solution (HEK)	140 mM CsF
	1mM EGTA
	10 mM NaCl
	10 mM HEPES

8.4 Primer sequences for genotyping

WT FW	5`GCCAGAGGCCACTTGTGTAG3`
Heterozygous	5`GCAAGTTGCCCTCZGACTTC3`
GLA KO	5`AGGTCCACAGCAAAGGATTG3`

8.5 Primer used for qRT-PCR

Table 4: Primer for qRT-PCR

Gene	Sequence 5´-3´	Assay-ID
TRPV1	not specified	Mm01246302_m1
HCN2	not specified	Mm00468538_m1
$Na_v1.7$	not specified	Mm00450762_s1
$Na_v1.8$	not specified	Mm00501467_m1
18s rRNA	not specified	Hs99999901_s1

8.6 Antibodies used in immunohisto-/cytochemistry

Table 5: Primary antibodies

Reactivity	Host	Company	Catalog #	Dilution	Fixation / Additives
β-III-Tubulin	Chicken	Abcam	ab41489	1:500	Acetone/ 0.3% Triton
CD77	Rat	Bio-Rad	MCA579	1:250	Acetone/ 0.3% Triton
HCN2	Rabbit	Alomone labs	APC-030	1:200	Acetone/ 0.03% Triton
Nav1.7	Rabbit	Alomone labs	ASC-008	no signal	Acetone/ 0.3% Triton

Nav1.7	Rabbit	Alomone labs	ASC-027	no signal	Acetone/ 0.3% Triton
Nav1.7	Guinea pig	Alomone labs	AGP-057	no signal	Acetone/ 0.3% Triton
Nav1.7	Mouse	Abcam	ab85015	no signal	Acetone/ 0.3% Triton
Nav1.7	Rat	Yale Medical school	Y083	no signal	Acetone/ 0.3% Triton
Nav1.8	Rabbit	Bio-Rad	AB9274	1:100	Acetone/ 0.3% Triton
TRPV1	Goat	Santa Cruz	SC-12498	1:500	Acetone/ 0.3% Triton

Table 6: Secondary antibodies

Reactivity	Host	Company	Catalog #	Dilution	Fixation / Additives
Alexa Fluor 488 anti-rat IgM	Goat	Jackson Laboratory	112-005-075	1:300	/
Cyanine 3.18 fluorescent probe anti rabbit	Goat	Amersham	PA63101	1:50	/
Cyanine 3.18 fluorescent probe anti goat	Rabbit	Amersham	PA63101	1:50	/

9. Abbreviations

α-Gal A	α-galactosidase A
BSA	bovine serum albumin
C57BL/6	C57 black 6
cAMP	cyclic adenosine monophosphate
CCI	chronic constriction injury
CD	cluster of differentiation
cDNA	complementary deoxyribonucleic acid
CFA	complete Freund`s adjuvant
Cy3	cyanine 3.18 fluorescent probe
DNA	deoxyribonucleic acid
CNS	central nervous system
DRG	dorsal root ganglion
ELISA	enzyme-linked immunosorbent assay
EPM	elevated plus maze
ER	endoplasmatic reticulum
ERT	enzyme replacement therapy
FD	Fabry disease
FST	forced swim test
Gb3	globotriaosylceramide
GLA KO	α-galactosidase A deficient mouse
HCN2	hyperpolarization-activated cyclic nucleotide-gated channel 2
HEK	human embryonic kidney 293 cells
IBM	international business machines
LDB	light-dark box

mRNA	messenger ribonucleic acid
MWM	Morris water maze
NaCl	sodium chloride
$Na_v1.7$	voltage-gated sodium channel 1.7
$Na_v1.8$	voltage-gated sodium channel 1.8
$Na_v1.9$	voltage-gated sodium channel 1.9
NGF	nerve growth factor
OF	open field
PBS	phosphate-buffered saline
PCR	polymerase chain reaction
PI(3)P	phosphatidylinositol 3-phosphate
PNS	peripheral nervous system
PKA	protein kinase A
p value	probability value
qRT-PCR	quantitative real-time polymerase chain reaction
QST	quantitative sensory testing
RNA	ribonucleic acid
SFN	small fiber neuropathy
shRNA	short hairpin ribonucleic acid
siRNA	short interferring ribonucleic acid
SPSS	statistical package of the social sciences
TRP	transient receptor potential
TRPV1	transient receptor potential vanilloid 1
WML	white matter lesions
WT	wildtype

10. List of Figures

11. List of Tables

12. Curriculum vitae

13. Publications

Original articles

Hofmann L, Karl F, Sommer C, Üçeyler N (2017). Affective and cognitive behavior in the alpha-galactosidase A deficient mouse model of Fabry disease. PLoS One. 12, e0180601.

Üçeyler N, Biko L, Hose D, **Hofmann L**, Sommer C (2016). Comprehensive and differential long-term characterization of the alpha-galactosidase A deficient mouse model of Fabry disease focusing on the sensory system and pain development. Mol Pain. 12.

Poster presentations at international conferences

Hofmann L, Grießhammer A, Sommer C, Wischmeyer E, Üçeyler N (2017). Behavioral, histological, and molecular characterization of the alpha-galactosidase A deficient mouse as a model of Fabry disease. 6th International congress on Neuropathic Pain, Gothenburg, Sweden

Hofmann L, Hose D, Sommer C, Wischmeyer E, Üçeyler N (2016). Pain in Fabry disease, the α-galactosidase A knock-out mouse as a model. 11th International symposium EUREKA, Würzburg, Germany

Hofmann L, Hose D, Grießhammer A, Sommer C, Wischmeyer E, Üçeyler N (2016). Behavioral, histological, and molecular characterization of the alpha-galactosidase A deficient mouse as a model of Fabry disease. 16th World Congress on Pain, Yokohama, Japan

14. Danksagung

Mein größter Dank geht an Frau Prof. Nurcan Üçeyler und Herrn Prof. Erhard Wischmeyer für die Überlassung der Doktorarbeit und natürlich dafür, dass ihr mir immer mit Rat und Tat zur Seite gestanden habt. Vielen Dank für alles, ich habe sehr viel von euch beiden gelernt.

Sehr herzlich möchte ich ebenfalls Frau Prof. Claudia Sommer und Frau Prof. Carmen Villmann für Ihre Beteiligung in meinem GSLS Promotionskomitee und die äußerst hilfreiche und konstruktive Kritik im Verlauf der letzten drei Jahre danken, ohne die eine erfolgreiche Promotion nicht möglich gewesen wäre.

Franziska, Thomas und Dimitar, tausend Dank für die tolle Zeit im Büro und neben der Arbeit. Danke für eure Unterstützung, sowohl moralisch, als auch wissenschaftlich. Ohne euch hätte ich die Arbeit niemals so durchführen können, Danke.

Vielen, vielen Dank an Lydia, Helga und Katharina für eure Unterstützung bei allem, was mit den Mäusen zu tun hatte. Außerdem natürlich Dankeschön für die schönen Kaffeepausen, bei denen man immer neue Energie und Motivation tanken konnte.

Ein herzliches Dankeschön geht ebenfalls an alle technischen Mitarbeiterinnen für die herzliche Aufnahme in die Arbeitsgruppe und in den Laboralltag, sowie für eure ständige Hilfsbereitschaft.

Des Weiteren möchte ich den Tierpflegern für ihren ständigen Einsatz zum Wohle der Tiere und Ihre Unterstützung bei meinen Versuchen danken. Weiterhin gilt Katharina Gerber ein großer Dank für ihre Hilfe bei meiner Einarbeitung für die Patch-clamp Analyse, sowie bei den Klonierungsexperimenten.

Nicht zu Letzt Danke ich meiner Familie, Freundin und Freunden für eure Hilfe, Geduld, Fürsorge und Unterstützung. Ohne einen solchen Rückhalt wäre es mir mit Sicherheit nicht möglich gewesen diese Arbeit in einer solchen Art und Weise durch zu führen und ab zu schließen.